Neuroscience

Homeostatic regulation of REM sleep by the preoptic area of the hypothalamus

Reviewed Preprint

Published from the original preprint after peer review and assessment by eLife.

About eLife's process

Reviewed preprint version 1
December 20, 2023 (this version)

Sent for peer review
August 31, 2023

Posted to preprint server
August 23, 2023

John Maurer, Alex Lin, Xi Jin, Jiso Hong, Nicholas Sathi, Romain Cardis, Alejandro Osorio-Forero, Anita Lüthi, Franz Weber, Shinjae Chung

Department of Neuroscience, Chronobiology and Sleep Institute, Perelman School of Medicine, University of Pennsylvania, Philadelphia, PA 19104, USA • Department of Fundamental Neurosciences, University of Lausanne, Rue du Bugnon 9, CH-1005 Lausanne, Switzerland

Abstract

Rapid-eye-movement sleep (REMs) is characterized by activated electroencephalogram (EEG) and muscle atonia, accompanied by vivid dreams. REMs is homeostatically regulated, ensuring that any loss of REMs is compensated by a subsequent increase in its amount. However, the neural mechanisms underlying the homeostatic control of REMs are largely unknown. Here, we show that GABAergic neurons in the preoptic area of the hypothalamus projecting to the tuberomammillary nucleus ($POA^{GAD2} \rightarrow TMN$ neurons) are crucial for the homeostatic regulation of REMs. $POA^{GAD2} \rightarrow TMN$ neurons are most active during REMs, and inhibiting them specifically decreases REMs. REMs restriction leads to an increased number and amplitude of calcium transients in $POA^{GAD2} \rightarrow TMN$ neurons, reflecting the accumulation of REMs pressure. Inhibiting $POA^{GAD2} \rightarrow TMN$ neurons during REMs restriction blocked the subsequent rebound of REMs. Our findings reveal a hypothalamic circuit whose activity mirrors the buildup of homeostatic REMs pressure during restriction and that is required for the ensuing rebound in REMs.

eLife assessment

This **valuable** study advances our understanding of the brain nuclei involved in rapid-eye movement (REM) sleep regulation. Using a combination of imaging, electrophysiology, and optogenetic tools, the study provides **convincing** evidence that inhibitory neurons in the preoptic area of the hypothalamus influence REM sleep. This work will be of interest to neurobiologists working on sleep and/or brain circuitry.

Introduction

REMs is homeostatically regulated as demonstrated in various species including mice, rats, cats and humans (Siegel and Gordon, 1965; Beersma et al., 1990; Benington et al., 1994; Endo et al., 1997, 1998; Rechtschaffen et al., 1999; Franken, 2002; Shea et al., 2008). REMs

restriction leads to an increased homeostatic need for REMs. During the subsequent recovery sleep, the amount of REMs is increased to compensate for the amount lost during restriction. While seminal dissection studies indicate a pontine origin of REMs, recent studies have revealed that neural populations in the hypothalamus, midbrain, amygdala and medulla regulate REMs by promoting or inhibiting REMs (Clément et al., 2011; Jego et al., 2013; Hayashi et al., 2015; Van Dort et al., 2015; Weber et al., 2015, 2018; Chung et al., 2017; Torontali et al., 2019). However, we do not have a clear understanding about the homeostatic mechanisms regulating REMs and which brain regions integrate homeostatic REMs pressure.

The preoptic area of the hypothalamus (POA) is crucial for sleep regulation. The POA contains neurons that become activated during sleep and that are sufficient and necessary for sleep (Von Economo, 1930; Nauta, 1946; McGinty and Sterman, 1968; Sallanon et al., 1989; Sherin et al., 1996; Szymusiak et al., 1998; Lu et al., 2000; Gong et al., 2004; Takahashi et al., 2009; Zhang et al., 2015; Kroeger et al., 2018). Specifically, POA GABAergic neurons projecting to the tuberomammillary nucleus ($POA^{GAD2}\rightarrow TMN$ neurons) form a subpopulation of sleep-active POA neurons, and promote sleep when optogenetically activated (Chung et al., 2017). A previous study demonstrated that c-Fos expression in the POA is increased in REMs restricted rats (Gvilia et al., 2006). However, the molecular identity of POA neurons that become activated during heightened REMs pressure and whether their activity is necessary for homeostatic REMs regulation remains largely unknown.

In this study, using fiber photometry, we found that $POA^{GAD2}\rightarrow TMN$ neurons become gradually activated during non-rapid eye movement sleep (NREMs) before the onset of REMs and are most active during REMs. Optogenetic inhibition of $POA^{GAD2}\rightarrow TMN$ neurons significantly decreased REMs. We therefore hypothesized that the $POA^{GAD2}\rightarrow TMN$ neurons are well suited to encode homeostatic pressure for REMs. Using fiber photometry recordings combined with REMs restriction, we show that the activity of $POA^{GAD2}\rightarrow TMN$ neurons significantly increased during periods of heightened REMs pressure. Optogenetic inhibition of $POA^{GAD2}\rightarrow TMN$ neurons during REMs restriction prevented the subsequent increase of REMs during recovery sleep. Our findings identify a hypothalamic circuit regulating the homeostatic need for REMs.

Results

$POA^{GAD2}\rightarrow TMN$ neurons are most active during REMs

To monitor the population activity of $POA^{GAD2}\rightarrow TMN$ neurons *in vivo* during spontaneous sleep, we performed fiber photometry recordings. GAD2-Cre mice were injected with retrograde adeno-associated viruses (AAVs) encoding Cre-inducible GCaMP8s (AAVretro-FLEX-jGCaMP8s) into the TMN (Tervo et al., 2016; Zhang et al., 2023), and an optic fiber was implanted into the POA (**Fig. 1A**). The calcium activity of $POA^{GAD2}\rightarrow TMN$ neurons was significantly higher during REMs compared with that during wake and NREMs (**Fig. 1B, C**; detailed statistical results are shown in **Figure legends** and **Table S1**).

We further analyzed the activity changes of the $POA^{GAD2}\rightarrow TMN$ neurons during NREMs→REMs or NREMs→wake transitions. We found that the calcium activity of $POA^{GAD2}\rightarrow TMN$ neurons during NREMs→ REMs transitions becomes significantly increased 40 s before the REMs onset and remains elevated throughout REMs (**Fig. 1D**). During NREMs→wake transitions, the activity of $POA^{GAD2}\rightarrow TMN$ neurons started rising 10 s before the wake onset and remained elevated for 10 s after the onset (**Fig. 1D**). The ΔF/F activity gradually increased throughout NREMs episodes (**Fig. 1E**).

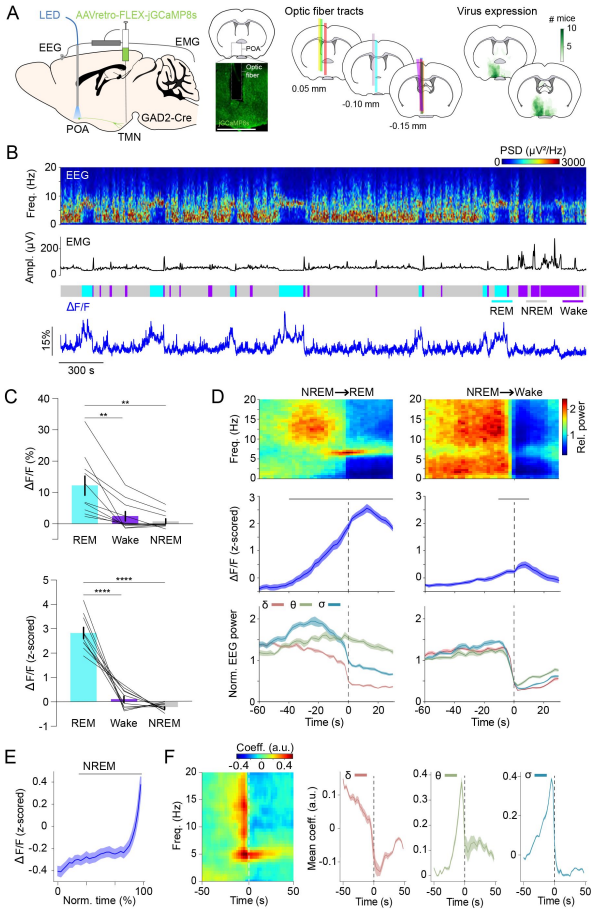

FIGURE 1.

POA^{GAD2}→TMN neurons are most active during REMs.

(A) Left, schematic of fiber photometry with simultaneous EEG and EMG recordings. Mouse brain figure adapted from the Allen Reference Atlas - Mouse Brain (*atlas.brain-map.org*). Center left, fluorescence image of POA in a GAD2-Cre mouse injected with AAVretro-FLEX-jGCaMP8s into the TMN. Scale bar, 1 mm. Center right, location of fiber tracts. Each colored bar represents the location of optic fibers for photometry recordings. Right, heatmaps outlining areas with cell bodies expressing GCaMP8. The green color code depicts how many mice the virus expression overlapped at the corresponding location (n = 10 mice).
(B) Example fiber photometry recording. Shown are EEG spectrogram, EMG amplitude, color-coded brain states, and ΔF/F signal.
(C) Non-normalized and z-scored ΔF/F activity during REMs, wake, and NREMs. Bars, averages across mice; lines, individual mice; error bars, ± s.e.m. One-way repeated measures (rm) ANOVA, p = 9e-4, 2e-6 for non-normalized ΔF/F and z-scored ΔF/F signals; pairwise t-tests with Bonferroni correction, non-normalized ΔF/F, p = 0.0056, 0.0039 for REMs vs. Wake and REMs vs. NREMs; z-scored ΔF/F, p = 6e-5, 1e-7. n = 10 mice.
(D) Average EEG spectrogram (top), z-scored ΔF/F activity (middle) and normalized EEG δ, θ and σ power (bottom) during NREMs→REMs transitions (left) and NREMs→Wake transitions (right). Shading, ± s.e.m. One-way rm ANOVA, p = 3.18e-49, 9.50e-8 for NREMs→REMs and NREMs→Wake; pairwise t-tests with Holm-Bonferroni correction, NREMs→REMs p < 0.0419 between -40 s and 30 s, NREMs→Wake p < 0.0106 between -10 s and 10 s. Gray bar, period when ΔF/F activity was significantly different from baseline (-60 to -50 s). n = 10 mice.
(E) ΔF/F activity during NREMs. The duration of NREMs episodes was normalized in time, ranging from 0 to 100%. Shading, ± s.e.m. Pairwise t-tests with Holm-Bonferroni correction p < 8.14e-9 between 20 and 100. Gray bar, intervals where ΔF/F activity was significantly different from baseline (0 to 20%, the first time bin). n = 566 events.
(F) Left, linear filter mapping the normalized EEG spectrogram onto the POA^{GAD2}→TMN neural activity. Time point 0 s corresponds to the predicted neural activity. Right, coefficients of the linear filter for δ, θ and σ power band. Shading, ± s.e.m. See **Table S1** for the actual p values.

Given that both the θ and σ (6-9 and 10.5-16 Hz) power increased preceding the REMs onset (**Fig. 1D**), we investigated the relationship between the POA^{GAD2}→TMN neuron activity and the spectral composition of the EEG in more detail (**Fig. 1F**). We used a linear regression model to predict the current POA^{GAD2}→TMN neural activity based on the preceding and following spectral EEG features (Weber et al., 2010; Schott et al., 2023). We found that the activity of POA^{GAD2}→TMN neurons is preceded by an increase in the θ and σ power and reduction in the δ (0.5-4.5 Hz) power (**Fig. 1F**). These changes in the EEG are characteristic for the stage of NREMs preceding REMs (Gottesmann, 1996) and their correlation with the activity of POA^{GAD2}→TMN neurons is consistent with a role of these neurons in promoting NREMs to REMs transitions.

In a complementary experiment, we monitored the calcium activity of POA^{GAD2}→TMN axonal fibers. GAD2-Cre mice were injected with AAV-FLEX-GCaMP6s into the POA and an optic fiber was implanted into the TMN (**Fig. S1A**). Similar to the activity found for POA^{GAD2}→TMN neurons using retrograde AAVs (**Fig. 1B, C**), POA^{GAD2}→TMN fibers were most active during REMs (**Fig. S1B, C**). During NREMs, the activity of POA^{GAD2}→TMN axonal fibers gradually increased before transitioning to REMs (**Fig. S1D**), demonstrating that the activity of POA^{GAD2}→TMN axonal fibers closely resembles that of cell bodies. In summary, these results demonstrate that the activity in POA^{GAD2}→TMN neurons increases prior to the onset of REMs episodes, following an increase in the θ and σ power in the EEG.

The TMN contains histamine neurons (TMN^{HIS}), and previous studies showed that POA^{GAD2} neurons innervate TMN^{HIS} neurons (Chung et al., 2017; Saito et al., 2018). Consistent with previous electrophysiological studies (Steininger et al., 1999; Vanni-Mercier et al., 2003; John et al., 2004; Takahashi et al., 2006), we found in photometry recordings that TMN^{HIS} neurons are highly active during wake and less active during NREMs and REMs (**Fig. S2A-C**). Consistent with this, the activity of TMN^{HIS} neurons became significantly activated after the transition from NREMs or REMs to wakefulness (**Fig. S2D**). The TMN^{HIS} neuron activity gradually decreased during NREMs episodes (**Fig. S2E**), possibly as a result of inhibitory inputs from POA^{GAD2}→TMN neurons (Chung et al., 2017).

Inhibiting POA^{GAD2}→TMN neurons reduces REMs

To examine whether POA^{GAD2}→TMN neurons regulate REMs, we optogenetically inhibited these neurons using the bistable chloride channel SwiChR++ (Berndt et al., 2016; Smith et al., 2022; Stucynski et al., 2022). GAD2-Cre mice were bilaterally injected with retrograde AAVs encoding Cre-inducible SwiChR++ (AAVretro-DIO-SwiChR++-eYFP) or eYFP (AAVretro-DIO-eYFP) into the TMN followed by bilateral optic fiber implantation into the POA (**Fig. 2A**). We compared SwiChR++ and eYFP recordings with and without laser stimulation (473 nm, 2 s step pulses at 60 s intervals for 3 h, zeitgeber time [ZT] 2-5). SwiChR++-mediated inhibition of POA^{GAD2}→TMN neurons reduced the amount of REMs compared with recordings without laser stimulation in the same mice and eYFP mice with laser stimulation (**Fig. 2B, C**). The overall time spent in wake and NREMs was not altered by SwiChR++-mediated inhibition (**Fig. 2C, S3A, B**) suggesting that POA^{GAD2}→TMN neuron activity specifically regulates the amount of REMs.

Next, we compared the spectral composition of the EEG throughout recordings with or without laser stimulation in SwiChR++ and eYFP mice. During REMs, SwiChR++-mediated inhibition of POA^{GAD2}→TMN neurons increased the δ and σ power in the EEG compared with SwiChR++-without laser and eYFP-laser groups (**Fig. 2D, S3C**). The δ, θ, and σ power in the EEG during NREMs and wake was indistinguishable between SwiChR++ and eYFP groups (**Fig. S3D**).

Next, we investigated the effect of sustained inhibition of POA^{GAD2}→TMN neurons on the following 3 h recording without laser stimulation (**Fig. 2E**). Despite the reduction of REMs during the laser stimulation in SwiChR++ mice (**Fig. 2C**), there were no differences in the amount of REMs, NREMs, and wake between SwiChR++ and eYFP groups during the post laser

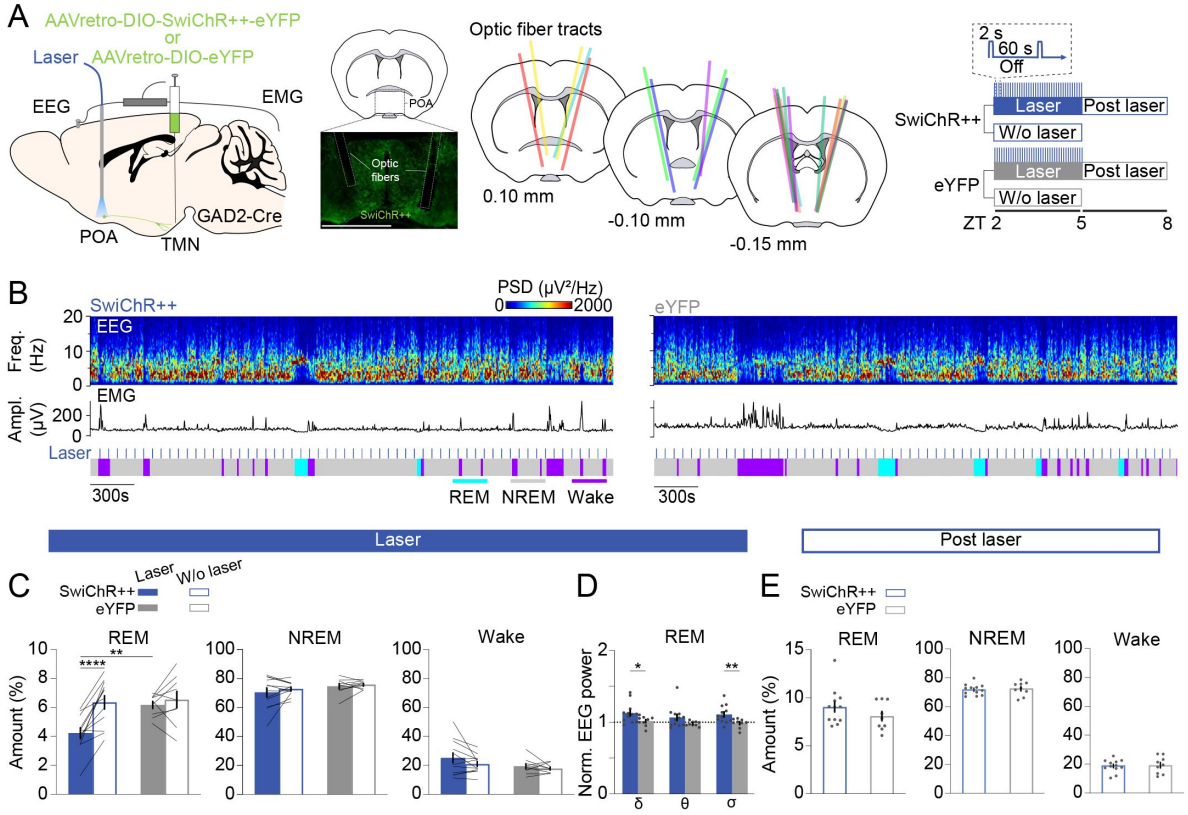

FIGURE 2.

Inhibiting POA^{GAD2}→TMN neurons reduces REMs.

(A) Left, schematic of optogenetic inhibition experiments. Center left, fluorescence image of POA in a GAD2-CRE mouse injected with AAVretro-DIO-SwiChR++-eYFP into the TMN. Scale bar, 1 mm. Center right, location of optic fiber tracts. Each colored bar represents the location of an optic fiber. Right, experimental paradigm for laser stimulation (2 s step pulses at 60 s intervals) in SwiChR++ and eYFP-expressing mice.
(B) Example recording of a SwiChR++ (left) and eYFP mouse (right) with laser stimulation. Shown are EEG power spectra, EMG amplitude, and color-coded brain states.
(C) Percentage of time spent in REMs, NREMs and wakefulness with and without laser in SwiChR++ and eYFP mice. Mixed ANOVA, virus p = 0.0629, laser p = 0.0003, interaction p = 0.0064; t-tests with Bonferroni correction, SwiChR-laser vs. SwiChR-w/o laser p = 3.00e-5, SwiChR-laser vs. eYFP-laser p = 0.0058.
(D) Normalized EEG δ, θ, and σ power during REMs in SwiChR++ and eYFP mice with laser. Unpaired t-tests, SwiChR vs. eYFP p = 0.0432, 0.0099 for δ and σ.
(E) Percentage of time spent in REMs, NREMs, and wakefulness during post laser sessions.
(C) Bars, averages across mice; lines, individual mice; error bars, ± s.e.m.
(D, E) Bars, averages across mice; dots, individual mice; error bars, ± s.e.m.
SwiChR++: n = 12 mice; eYFP: n = 9 mice

recordings (**Fig. 2E, S3E, F**), suggesting that the loss of REMs during SwiChR++-mediated inhibition was not followed by a homeostatic increase in REMs. Taken together, we first demonstrated that SwiChR++-mediated inhibition of $POA^{GAD2}\rightarrow$TMN neurons reduced the amount of REMs, supporting a necessary role of these neurons in REMs regulation. Second, the lost amount of REMs was not compensated for in the subsequent sleep suggesting that their activity is involved in the homeostatic regulation of REMs.

$POA^{GAD2}\rightarrow$TMN neurons exhibit an increased number of calcium transients during REMs restriction

To probe whether the activity of $POA^{GAD2}\rightarrow$TMN neurons changes during periods of high REMs pressure resulting from REMs restriction, we performed fiber photometry recordings combined with a closed-loop REMs restriction protocol (**Fig. 3A**). To detect the onset of REMs, we adapted a previously applied automatic REMs detection algorithm (Weber et al., 2015, 2018; Stucynski et al., 2022; Schott et al., 2023). Briefly, the animal's brain state was classified based on real-time analysis of the EEG/EMG signals. As soon as a REMs episode was detected, a small vibrating motor attached to the animal's head was turned on to terminate REMs by briefly awakening the animal (**Fig. 3A, S4A**) (Cardis et al., 2021; Osorio-Forero et al., 2023). Compared with the baseline recordings from the same mice during the same circadian time, we found that 6 h of REMs restriction (ZT 1.5-7.5) significantly reduced the amount of REMs and duration of REMs episodes, while increasing their frequency (**Fig. S4A, D-F**). The number of motor activations gradually increased as mice tried to enter REMs more frequently, indicating the accumulation of REMs pressure (**Fig. S4B**). Before the onset of the motor vibration, we found a clear increase in the EEG θ band reflecting NREMs to REMs transitions (**Fig. S4C**). We also investigated the effects of REMs restriction on the spectral composition of the EEG. We found an increased δ power for REMs during restriction (**Fig. S4G**). During rebound (ZT 7.5-8.5), the amount of REMs was significantly increased compared with that during the same circadian time due to an increased frequency of REMs episodes (**Fig. S4H-K**), compensating for the amount of REMs lost during restriction.

During REMs restriction, we observed an increased number of calcium transients in the activity of $POA^{GAD2}\rightarrow$TMN neurons as the REMs pressure increased (**Fig. 3A, B**). To detect and quantify these transients, we applied an algorithm previously applied to detect calcium events in fiber photometry recordings (Antila et al., 2022; Smith et al., 2022). Using fiber photometry, we monitored the population activity of $POA^{GAD2}\rightarrow$TMN neurons during the last hour of REMs restriction (ZT 6.5-7.5, referred as Restr.) and the first hour of REMs rebound (ZT 7.5-8.5, referred as Reb.) and compared it with the activity during baseline recordings of the same mice on separate days at the same circadian time (**Fig. 3A, B**). To restrict REMs, we used a motor (ZT 1.5-5.5) as previously described or gently pulled a string attached to the animal's head (ZT 5.5-7.5) during the photometry recordings (**Fig. 3A**). We verified that REMs was adequately restricted (**Fig. S5**). During restriction, the number of calcium transients of the $POA^{GAD2}\rightarrow$TMN neurons was significantly increased compared with that during baseline recordings (**Fig. 3C**). In particular, the number of calcium peaks was significantly elevated during NREMs, likely reflecting an increased pressure to transition to REMs (**Fig. 3C**). As the duration of REMs episodes was largely reduced as a result of the restriction (**Fig. S5A**), the number of peaks during REMs was not changed.

We further examined the amplitude of calcium transients during both NREMs and REMs. During REMs restriction, the amplitude of NREMs and REMs calcium transients was significantly higher compared with that during the circadian baseline (**Fig. 3D, E**) and remained elevated during NREMs in the rebound phase (**Fig. 3F, G**). Overall, these findings show that during periods of high REMs pressure, the $POA^{GAD2}\rightarrow$TMN neurons exhibit an increased number of calcium transients with higher amplitude compared with that during baseline levels suggesting that the activity of these neurons may reflect the heightened homeostatic need for REMs.

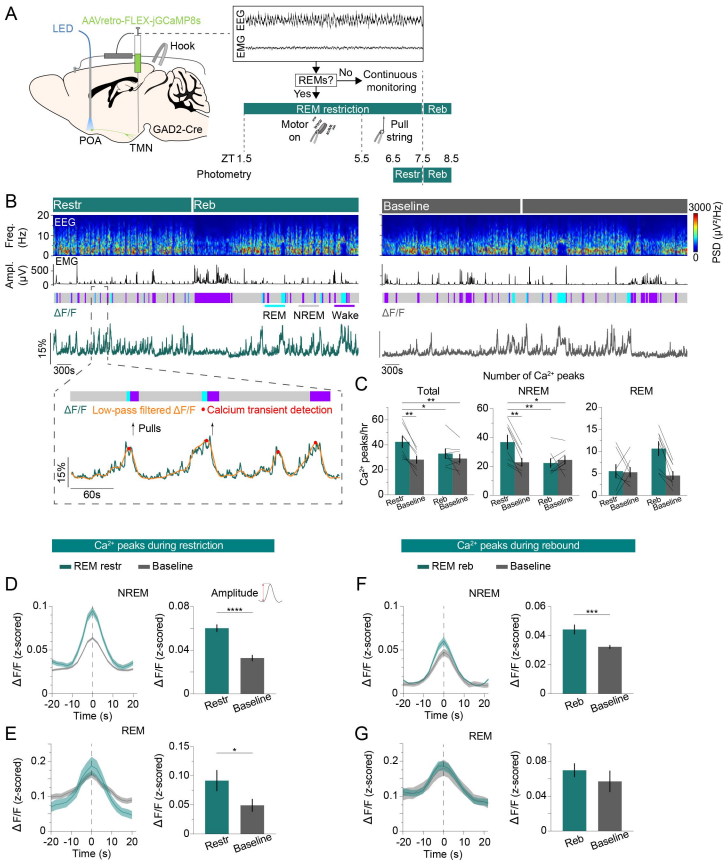

FIGURE 3.

POA^{GAD2}→TMN neurons exhibit an increased number of calcium transients during REMs restriction.

(A) Schematic of REMs restriction/rebound and photometry recording experiments. The brain state was continuously monitored; once a REMs episode was detected, we used a vibrating motor (ZT 1.5-5.5) or pulled a string (ZT 5.5-7.5) attached to the mouse head to terminate REMs. Fiber photometry recordings were performed during REMs restriction (ZT 6.5-7.5) and rebound (ZT 7.5-8.5).

(B) Top, example fiber photometry recording. Shown are EEG spectrogram, EMG amplitude, color-coded brain states, and ΔF/F signal. Bottom, brain states, ΔF/F signal (green), low-pass filtered ΔF/F signal (orange), detected peaks (red) and pulls (arrows) during a selected interval (dashed box) at an expanded timescale.

(C) Number of calcium peaks during all states (left), NREMs (middle) and REMs (right). Bars, averages across mice; lines, individual mice; error bars, ± s.e.m. n = 8 mice.

Total: two-way rm ANOVA, treatment (baseline vs. manipulation) p = 0.0031, time p = 0.0613, interaction p = 0.0189; t-tests with Bonferroni correction, REM restriction (restr.) vs. baseline (ZT 6.5-7.5) p = 0.0033, restr. vs. REM rebound (reb.) p = 0.0341, restr. vs. baseline (ZT 7.5-8.5) p = 0.0049.

NREMs: two-way rm ANOVA, treatment p = 0.0233, time p = 0.0363, interaction p = 0.003; t-tests with Bonferroni correction, restr. vs. baseline (ZT 6.5-7.5) p = 0.0057, restr. vs. reb. p = 0.0046, restr. vs. baseline (ZT 7.5-8.5) p = 0.0115.

(D) Left, average NREMs calcium peaks during REMs restriction and baseline recordings. Right, average amplitude of the NREMs calcium peaks. The amplitude was calculated by subtracting the ΔF/F value 10 s before the peak from its value at the peak. Unpaired t-tests, p = 6.30e-10. n = 295 and 196 peaks during restriction and baseline recordings.

(E) Left, average REMs calcium peaks during REMs restriction and baseline recordings. Right, average amplitude of the REMs calcium peaks. Unpaired t-tests, p = 0.0437. n = 44 and 42 peaks during restriction and baseline recordings.

(F) Left, average NREMs calcium peaks during REMs rebound and baseline recordings. Right, average amplitude of the NREMs calcium peaks. Unpaired t-tests, p = 0.0002. n = 180 and 196 peaks during rebound and baseline recordings.

(G) Left, average REMs calcium peaks during REMs rebound and baseline recordings. Right, average amplitude of the REMs calcium peaks. n = 84 and 36 peaks during rebound and baseline recordings.

(D-G) Bars, averages across trials; error bars, ± s.e.m; shadings, ± s.e.m.

Inhibition of POA^{GAD2}→TMN neurons during REMs restriction reduces the REMs rebound

To investigate whether the activity of POA^{GAD2}→TMN neurons encodes REMs pressure and consequently facilitates the subsequent rebound in REMs, we optogenetically inhibited these neurons during the last 3 h of REMs restriction. GAD2-Cre mice were bilaterally injected with retrograde AAVs encoding Cre-inducible SwiChR++ (AAVretro-DIO-SwiChR++-eYFP) or eYFP (AAVretro-DIO-eYFP) into the TMN followed by bilateral optic fiber implantation into the POA (**Fig. 4A**). Mice underwent REMs restriction (6 h, ZT 1.5-7.5), and laser stimulation (2 s step pulses at 60 s intervals) was applied during the last 3 hours (ZT 4.5-7.5), when the REMs pressure was highest (**Fig. S4B**). During restriction, SwiChR-mediated inhibition of POA^{GAD2}→TMN neurons decreased the percentage of REMs and reduced the frequency of REMs episodes with marginal significance (**Fig. 4B-D**, **S6A, B**). We found that inhibition of POA^{GAD2}→TMN neurons during REMs restriction resulted in a reduced amount of REMs during the rebound compared with that in eYFP mice (**Fig. 4B, F, G, S6D, E**). Thus, inactivating POA^{GAD2}→TMN neurons during heightened REMs pressure not only decreased the amount of REMs, but also prevented its homeostatic rebound during the following recovery sleep.

Finally, we examined the spectral composition of the EEG during the REMs restriction. We found that inhibition of POA^{GAD2}→TMN neurons during REMs restriction reduced the REMs δ power, NREMs θ and σ power compared with that in eYFP mice with laser stimulation (**Fig. 4E**, **S6C**). The reduced θ and σ power during NREMs could result from less attempts to enter REMs (**Fig. 4D**). During rebound, there were no significant differences in EEG δ, θ and σ power during REMs and NREMs (**Fig. 4H**, **S6F**).

Taken together, inhibiting POA^{GAD2}→TMN neurons during REMs restriction significantly decreased the amount of REMs and blocked the subsequent rebound in REMs. Our data suggest that the heightened activity of POA^{GAD2}→TMN neurons during sleep encodes the increased need for REMs and consequently plays an important role in the homeostatic response to REMs restriction.

Discussion

Our study demonstrates a role of POA^{GAD2}→TMN neurons in the homeostatic regulation of REMs. Using fiber photometry, we showed that the POA^{GAD2}→TMN neurons become activated throughout NREMs before transitioning to REMs, while being most active during REMs (**Fig. 1**). Sustained optogenetic inhibition of POA^{GAD2}→TMN neurons reduced the overall amount of REMs, and the loss of REMs was not compensated during the subsequent recovery sleep (**Fig. 2**). During the period of high REMs pressure, POA^{GAD2}→TMN neurons exhibited an increased number of calcium transients with elevated amplitude (**Fig. 3**). Optogenetic inhibition of POA^{GAD2}→TMN neurons during REMs restriction attenuated the subsequent rebound of REMs (**Fig. 4**). Our results suggest that the activity of POA^{GAD2}→TMN neurons reflects an increased need for REMs in the form of enhanced calcium transients and is required for the rebound following the loss of REMs.

The TMN contains histamine-producing neurons and antagonizing histamine signaling causes sleepiness (Watanabe et al., 1983; Panula et al., 1984; Lin et al., 1988; Bayliss et al., 1990; Haas et al., 2008). Consistent with our photometry recordings (**Fig. S2**), electrophysiological recordings demonstrate that TMN^{HIS} neurons are most active during wakefulness and less active during NREMs and REMs (Steininger et al., 1999; Vanni-Mercier et al., 2003; John et al., 2004; Takahashi et al., 2006). Throughout NREMs, the activity of TMN^{HIS} neurons gradually decreased while that of POA^{GAD2}→TMN neurons showed an opposite pattern (**Fig 1E**, **S2E**),

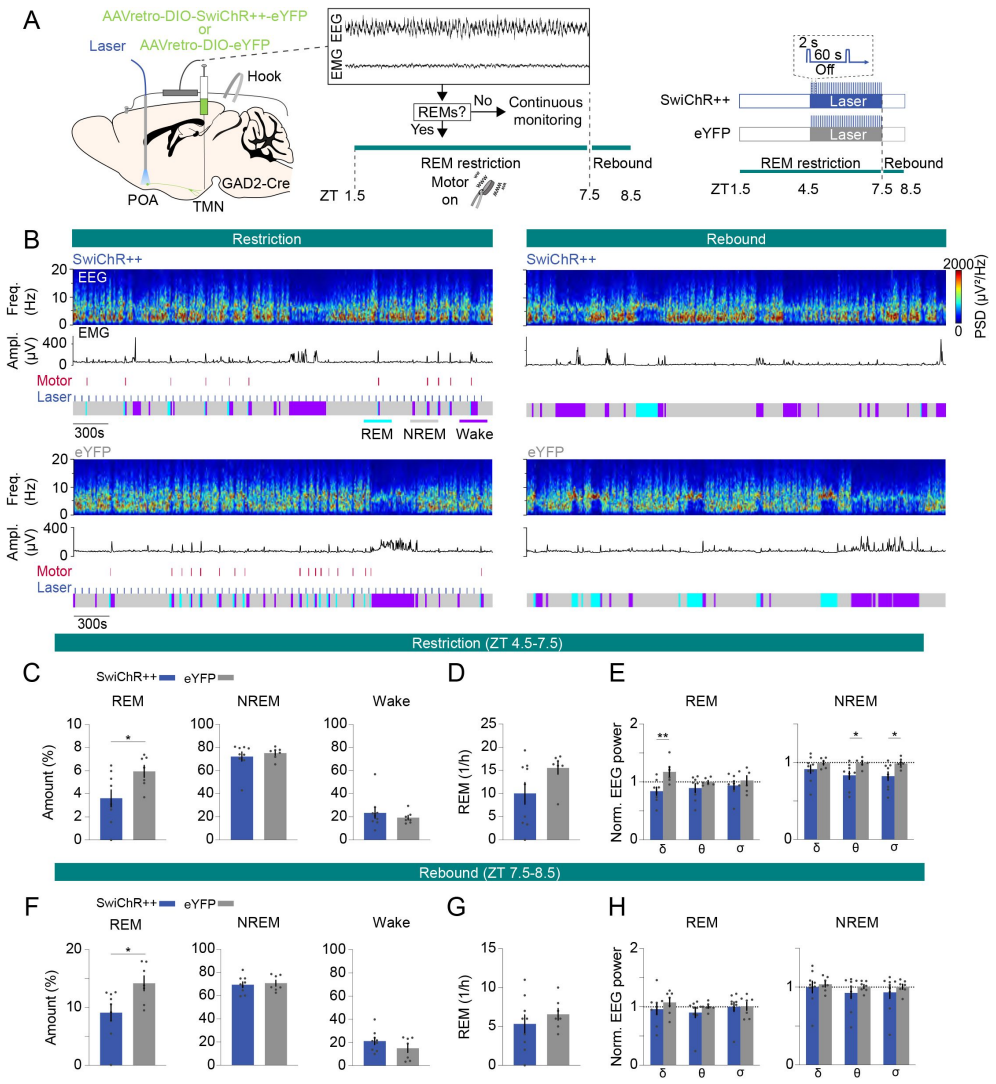

FIGURE 4.

Inhibition of POA^{GAD2}→TMN neurons during REMs restriction attenuates the REMs rebound.

(A) Schematic of REMs restriction/rebound and optogenetic inhibition experiments. During closed-loop REMs restriction (ZT 1.5-7.5), a vibrating motor attached to the mouse head was used to terminate REMs. REMs was restricted for 6 hours (ZT 1.5-7.5). During the last three hours of restriction (ZT 4.5-7.5), laser stimulation (2 s step pulses at 60 s intervals) was applied in SwiChR++ and eYFP mice.
(B) Example sessions from a SwiChR++ (top) and eYFP mouse (bottom) during REMs restriction with laser stimulation (left) and rebound (right). Shown are EEG spectrogram, EMG amplitude, motor vibration events, laser and color-coded brain states.
(C) Percentage of time spent in REMs, NREMs and wakefulness during the last 3 h of REMs restriction with laser stimulation (ZT 4.5-7.5) in mice expressing SwiChR++ and eYFP. Unpaired t-tests, p = 0.026 for REMs amount.
(D) Frequency of REMs episodes during the last 3 h of REMs restriction with laser stimulation. Unpaired t-tests, p = 0.0821.
(E) Normalized EEG δ, θ and σ power during the last 3 h of REMs restriction with laser stimulation. Unpaired t-tests, p = 0.0091, 0.0332, and 0.038 for REMs δ, NREMs θ and σ power.
(F) Percentage of time spent in REMs, NREMs and wakefulness during REMs rebound (ZT 7.5-8.5) in SwiChR++ and eYFP mice. Unpaired t-tests, p = 0.0205 for REMs amount.
(G) Frequency of REMs episodes during REMs rebound.
(H) Normalized EEG δ, θ and σ power during REMs rebound.
Bars, averages across mice; dots, individual mice; error bars, ± s.e.m.
SwiChR++: n = 9 mice; eYFP: n = 7 mice

which is likely in part the result of direct synaptic inputs from the POA^{GAD2}→TMN neurons to TMN^{HIS} neurons (Chung et al., 2017; Saito et al., 2018). TMN^{HIS} neurons in turn inhibit putative sleep-active POA neurons (Williams et al., 2014). Mutual inhibition between TMN^{HIS} and POA^{GAD2}→TMN neurons may explain their antagonistic activity pattern revealed in our fiber photometry recordings.

While many studies have focused on the role of the POA in regulating NREMs (Sherin et al., 1996; Szymusiak et al., 1998; Lu et al., 2000; Zhang et al., 2015; Kroeger et al., 2018; Ma et al., 2019), previous *in vivo* electrophysiological studies found that the majority of sleep-active neurons in the POA are most active during REMs (Osaka and Matsumura, 1995; Takahashi et al., 2009; Antila et al., 2022). Similarly, recent fiber photometry recordings demonstrated that GABAergic neurons in the POA and their subtypes expressing cholecystokinin, corticotropin-releasing hormone, tachykinin 1 or galanin are most active during REMs (Miracca et al., 2022; Smith et al., 2022). Deleting the NMDA receptor GluN1 subunit in the POA reduced REMs (Miracca et al., 2022), and in line with this, sustained optogenetic inhibition of POA^{GAD2}→TMN neurons specifically decreased REMs. Consistent with these studies, our findings also support an important role of the POA in REMs regulation and, in addition, provide evidence that these neurons are also part of the homeostat regulating REMs.

A previous study showed that the number of c-Fos positive POA neurons is positively correlated with the amount of REMs in rats (Lu et al., 2002). Moreover, REMs restriction led to an increase in the number of POA neurons expressing c-Fos, which was correlated with the number of attempts to enter REMs (Gvilia et al., 2006). Together with our findings that the number of calcium transients of POA^{GAD2}→TMN neurons increased during REMs restriction and that inhibition of these neurons blocked the following REMs rebound, these results support a crucial role of the POA in the homeostatic regulation of REMs. For the future, it would be interesting to test whether POA neurons projecting to other postsynaptic areas are also involved in the homeostatic regulation of REMs. A previous study showed that POA neurons projecting to REMs-regulatory pontine regions including the laterodorsal tegmental nucleus, locus coeruleus (LC) and dorsal raphe nucleus express increased levels of c-Fos after periods of dark exposure that increased REMs (Lu et al., 2002). However, the number of c-Fos positive POA neurons projecting to the LC was not increased upon REMs restriction, suggesting that this subpopulation may not be involved in the homeostatic regulation of REMs (Verret et al., 2006). Besides the TMN, the POA also projects to other REMs-regulatory regions such as the ventrolateral periaqueductal gray (vlPAG) and lateral hypothalamus (Steininger et al., 2001; Saito et al., 2018). Particularly, the projections to the vlPAG are of interest for future research, as GABAergic neurons in this area have been previously implicated in the homeostatic regulation of REMs (Hayashi et al., 2015; Weber et al., 2018).

The cellular mechanisms underlying the elevated activity of POA neurons during high REMs pressure are unknown. Sleep-promoting neurons in the dorsal fan-shaped body of *Drosophila* display increased intrinsic neuronal excitability in response to sleep need (Donlea et al., 2014). The elevated activity of POA^{GAD2}→TMN neurons during heightened REMs pressure may similarly be the result of an increased excitability. Given that the POA is also involved in the homeostatic regulation of NREMs (Sherin et al., 1996; Szymusiak et al., 1998; Gong et al., 2004; Zhang et al., 2015; Ma et al., 2019; Lu et al., 2000), it would be interesting to study how different POA subpopulations integrate the homeostatic need for NREMs and REMs.

Together, we have demonstrated a role of POA^{GAD2}→TMN neurons in the homeostatic regulation of REMs. REMs disturbances are observed in a variety of psychiatric disorders such as depression and PTSD and often precede their clinical onset (Ross et al., 1989; Gottesmann and Gottesman, 2007; Germain, 2013; Palagini et al., 2013). Elucidating the circuit mechanisms underlying

the homeostatic regulation of REMs may provide novel therapeutic targets to specifically regulate and normalize REMs in these psychiatric disorders to alleviate associated symptoms and potentially slow down their progression.

Materials and methods

Mice

All experimental procedures were approved by the Institutional Animal Care and Use Committee (IACUC reference # 806197) at the University of Pennsylvania and conducted in compliance with the National Institutes of Health Office of Laboratory Animal Welfare Policy. Experiments were performed in male and female GAD2-IRES-Cre mice (#010802, Jackson Laboratory) or HDC-IRES-Cre mice (#021198, Jackson Laboratory) aged 10-18 weeks, weighing 18-25 g at the time of surgery. Animals were group-housed with littermates on a 12h light/12h dark cycle (lights on 7 am and off 7 pm) with *ad libitum* access to food and water.

Viruses

Cre-dependent adeno-associated viral vectors were used to selectively express GCaMP, SwiChR++ or eYFP in POA^{GAD2} → TMN neurons, POA^{GAD2} → TMN projections or TMN^{HIS} neurons. pGP-AAV-Syn-FLEX-jGCaMP8s-WPRE (162377-AAVrg, Addgene) pAAV-Syn-FLEX-GCaMP6s-WPRE-SV40 (Penn Vector Core or 100845-AAV1, Addgene) $rAAV_2$-Retro–Ef1α-DIO-SwiChR++-eYFP (R47730, UNC Vector Core) $rAAV_2$-Retro–Ef1α-DIO-eYFP (R49556, UNC Vector Core).

Surgical procedures

All procedures followed the IACUC guidelines for rodent survival surgery. Mice were anesthetized with isoflurane (1-2%) during the surgery, and placed on a stereotaxic frame (Kopf) while being on a heating pad to maintain body temperature. The skin was incised and small holes were drilled for virus injections and implantations of optic fibers and EEG/EMG electrodes.

For fiber photometry experiments to image POA^{GAD2} → TMN neurons (**Fig. 1**, **3**), pGP-AAV-Syn-FLEX-jGCaMP8s-WPRE was injected (Nanoject II, Drummond Scientific) into the TMN (300 nl; AP -2.4 mm; ML -1 mm; DV -5.4 to -5.2 mm, relative to bregma) and an optic fiber (400 µm diameter) was implanted into the POA (AP 0.2 mm; ML -0.6 mm; DV -5.2 mm). For imaging the POA^{GAD2} → TMN axonal fibers (**Fig. S1**), pAAV-Syn-FLEX-GCaMP6s-WPRE-SV40 was injected into the POA (300 nl) and an optic fiber was implanted into the TMN. To image TMN^{HIS} neurons (**Fig. S2**), pAAV-Syn-FLEX-GCaMP6s-WPRE-SV40 was injected into the TMN (300 nl) and an optic fiber was implanted into the TMN.

For optogenetic inhibition experiments (**Fig. 2**, **4**), $rAAV_2$-Retro–Ef1α-DIO-SwiChR++-eYFP (for inhibition group) or $rAAV_2$-Retro–Ef1α-DIO-eYFP (for control group) was bilaterally injected into the TMN (300 nl) and bilateral optic fibers (200 µm diameter) were implanted into the POA (AP 0.2 mm; ML +/-1.5 mm [angled at 10°]; DV -5.2 mm).

All mice were implanted with electroencephalogram (EEG) and electromyogram (EMG) electrodes. EEG signals were recorded with stainless steel wires attached to two screws, located in the skull on top of the parietal (AP -2 mm; ML 2 mm) and frontal cortex (AP 1.7 mm; ML 0.6 mm). A reference screw was inserted on top of the cerebellum. Two EMG electrodes were inserted into the neck musculature. The incision was closed with suture and the EEG/EMG electrodes and optic fibers were secured to the skull using dental cement (A-M Systems). We performed optogenetic and fiber photometry experiments at least 4 wks after surgery.

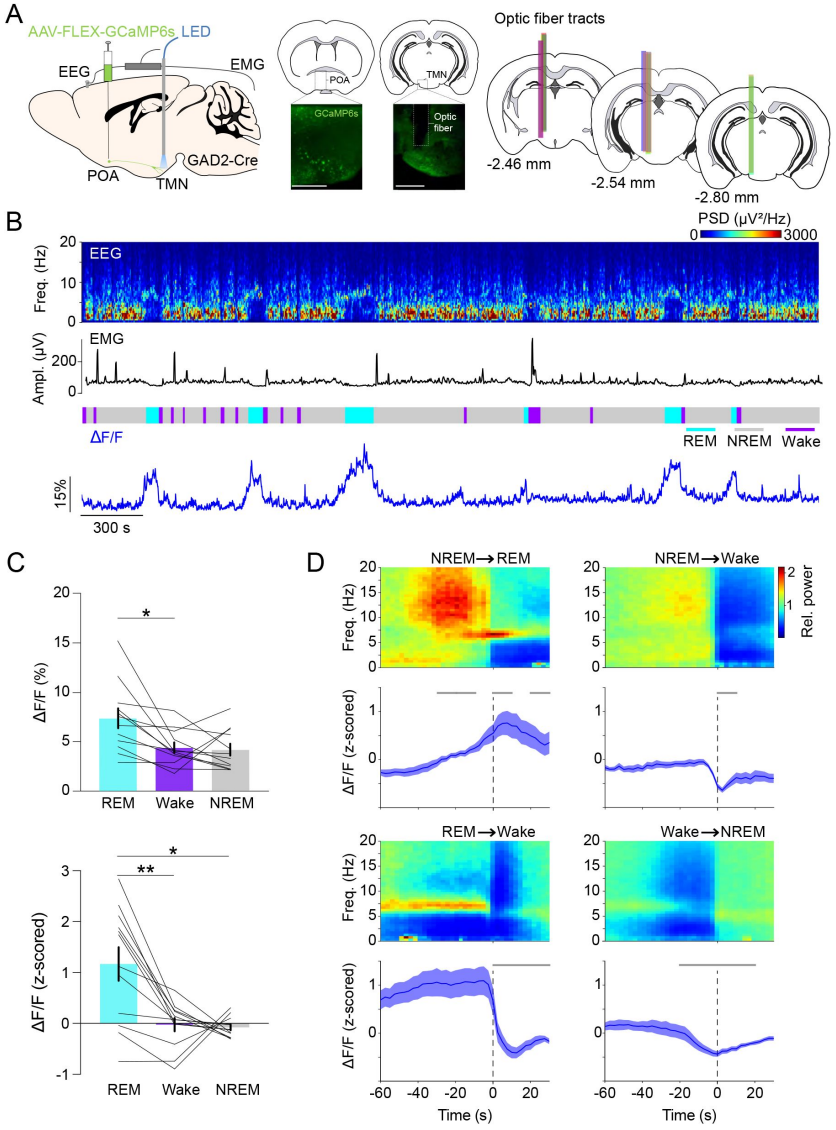

FIGURE S1.

POA^{GAD2}→TMN axonal fibers are most active during REMs. Related to Figure 1.

(A) Left, schematic of fiber photometry with simultaneous EEG and EMG recordings. Mouse brain figure adapted from the Allen Reference Atlas - Mouse Brain (*atlas.brain-map.org*). Middle, fluorescence image of POA and TMN in a GAD2-Cre mouse injected with AAV-FLEX-GCaMP6s into the POA and implanted with an optic fiber in the TMN. Scale bar, 0.5 mm. Right, location of fiber tracts. Each colored bar represents the location of optic fibers for photometry recordings.
(B) Example fiber photometry recording. Shown are EEG spectrogram, EMG amplitude, color-coded brain states, and ΔF/F signal.
(C) Non-normalized and z-scored ΔF/F activity during REMs, wake, and NREMs. Bars, averages across mice; lines, individual mice; error bars, ± s.e.m. One-way rm ANOVA p = 0.0162, 0.0029 for non-normalized ΔF/F and z-scored ΔF/F; pairwise t-tests with Bonferroni correction, non-normalized ΔF/F, p = 0.0187 for REMs vs. Wake; z-scored ΔF/F, p = 0.0018, 0.0227 for REMs vs. Wake or REMs vs. NREMs.
(D) Average EEG spectrogram (top), calcium activity (bottom) during brain state transitions. Shading, ± s.e.m. One-way rm ANOVA, p = 6.89e-8 for NREMs→REMs transitions; pairwise t-tests with Holm-Bonferroni correction, p < 0.0149 between -30 s and -10 s, p = 0.0002 between 0 and 10 s, p = 0.0361 between 20 and 30 s. Gray bar, period when ΔF/F activity was significantly different from baseline (-60 to -50 s).
n = 12 mice.
See **Table S1** for the actual p values.

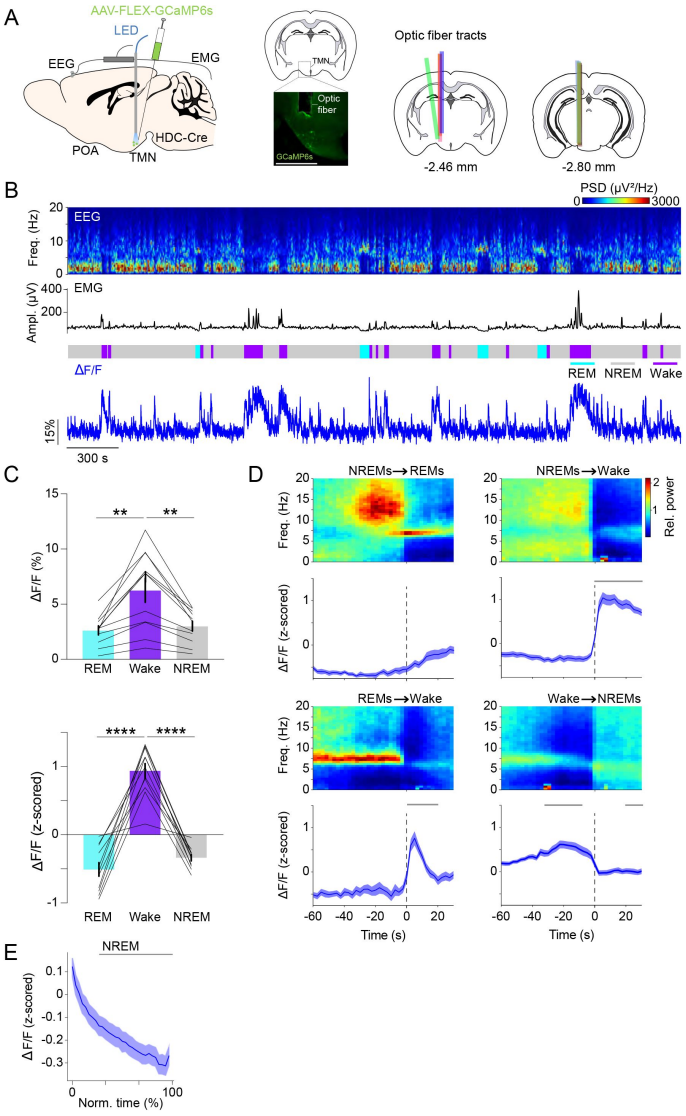

FIGURE S2.

TMN^{HIS} neurons are least active during sleep. Related to Figure 1.

(A) Left, schematic of fiber photometry with simultaneous EEG and EMG recordings. Middle, fluorescence image of TMN in a HDC-Cre mouse injected with AAV-FLEX-GCaMP6s and implanted with an optic fiber in the TMN. Scale bar, 1 mm. Right, location of fiber tracts. Each colored bar represents the location of optic fibers for photometry recordings.
(B) Example fiber photometry recording. Shown are EEG spectrogram, EMG amplitude, color-coded brain states, and ΔF/F signal.
(C) Non-normalized and z-scored ΔF/F activity during REMs, wake, and NREMs. Bars, averages across mice; lines, individual mice; error bars, ± s.e.m. One-way rm ANOVA p = 5.23e-4, 1.862e-11 for non-normalized ΔF/F and z-scored ΔF/F; pairwise t-tests with Bonferroni correction, non-normalized ΔF/F, p = 0.0035, 0.0022 for REMs vs. wake or wake vs. NREMs; z-scored ΔF/F, p = 2.95e-7, 3.81e-8. n = 11 mice.
(D) Average EEG spectrogram (top), and calcium activity (bottom) during brain state transitions. Shading, ± s.e.m. One-way rm ANOVA, p = 4.28e-40, 3.69e-22 for NREMs→wake and REMs→wake; pairwise t-tests with Holm-Bonferroni correction, NREMs→wake p < 1.44e-05 between 0 s and 30 s, REMs→wake p < 0.002 between 0 s and 20 s. Gray bar, period when ΔF/F activity was significantly different from baseline (-60 to -50 s). n = 11 mice.
(E) ΔF/F activity during NREMs. The duration of NREMs episodes was normalized in time, ranging from 0 to 100%. Shading, ± s.e.m. Pairwise t-tests with Holm-Bonferroni correction p < 5.36e-33 between 20 and 100. Gray bar, intervals where ΔF/F activity was significantly different from baseline (0 to 20%, the first time bin). n = 889 events.

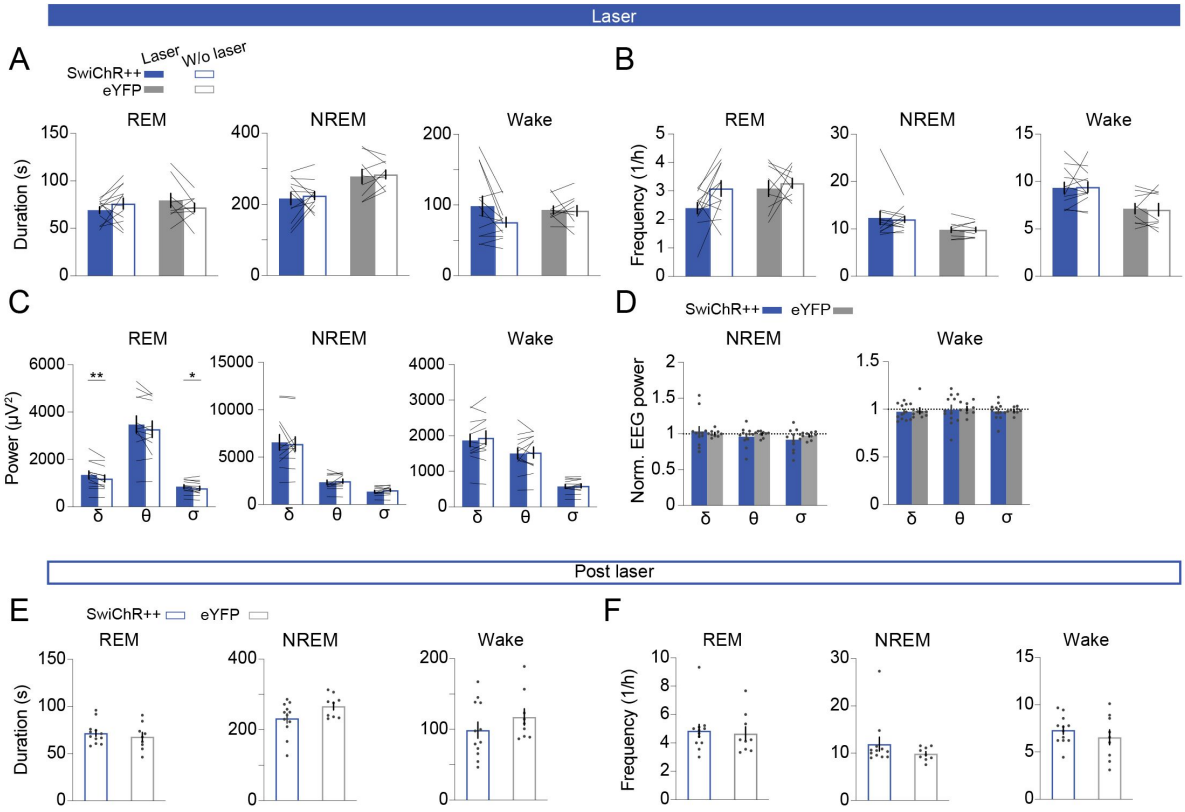

FIGURE S3.

Effects of inhibiting POA^{GAD2}→TMN neurons on brain states and EEG. Related to Figure 2.

(A) Duration of REMs, NREMs, and wake episodes with and without laser stimulation in SwiChR++ and eYFP mice.
(B) Frequency of REMs, NREMs, and wake episodes with and without laser stimulation in SwiChR++ and eYFP mice.
(C) Comparison of EEG δ, θ, and σ power during REMs, NREMs, and wakefulness with and without laser stimulation in SwiChR++ mice. Paired t-tests, SwiChR-laser vs. SwiChR-w/o laser p = 0.0048, 0.0158 for δ and σ during REM.
(D) Normalized EEG δ, θ, and σ power during NREMs, and wakefulness in SwiChR++ and eYFP mice.
(E) Duration of REMs, NREMs, and wake episodes during 3 h recordings directly following the laser stimulation interval (post laser) in SwiChR++ and eYFP mice.
(F) Frequency of REMs, NREMs, and wake episodes during post laser recordings in SwiChR++ and eYFP mice.
(A-C) Bars, averages across mice; lines, individual mice; error bars, ± s.e.m.
(D-F) Bars, averages across mice; dots, individual mice, error bars, ± s.e.m.
SwiChR++: n = 12 mice; eYFP: n = 9 mice

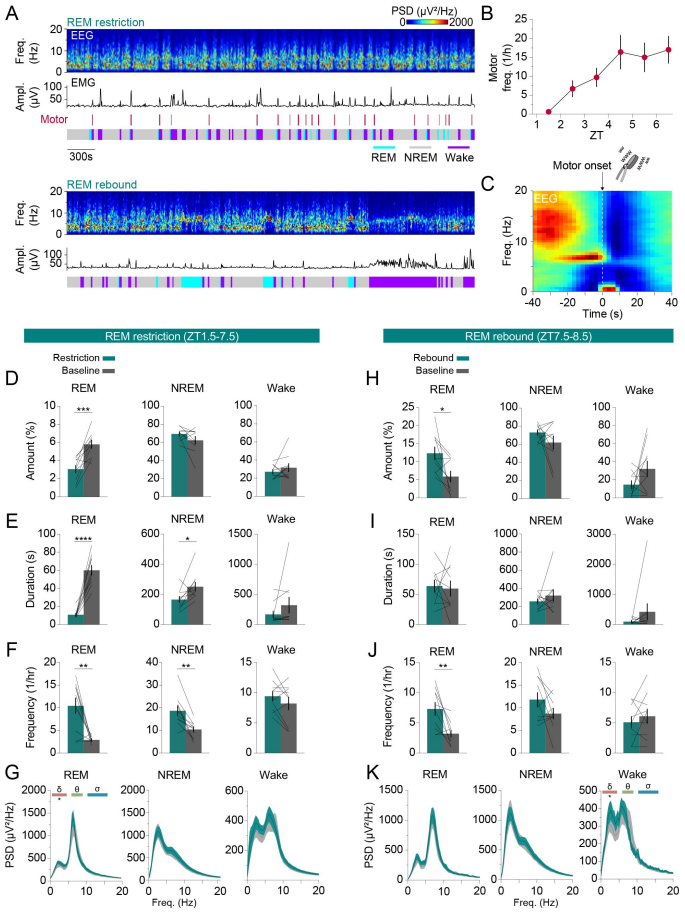

FIGURE S4.

Effects of REMs restriction on brain states and EEG. Related to Figure 3.

(A) Example session during REMs restriction (top) and REMs rebound (bottom) from the same mouse. Shown are EEG spectrogram, EMG amplitude, motor vibration events, and color-coded brain states.
(B) Frequency of motor vibration events throughout REMs restriction (ZT 1.5-7.5). Error bars, ± s.e.m. One way ANOVA p = 0.0061.
(C) Average normalized EEG spectrogram preceding motor vibration onset.
(D) Percentage of time spent in REMs, NREMs, and wakefulness during 6 h of REMs restriction (green, ZT 1.5-7.5) and baseline recordings (gray, ZT 1.5-7.5). Paired t-test, p = 0.0006 for REMs amount.
(E) Duration of REMs, NREMs, and wake episodes during 6 h of REMs restriction (green) and baseline recordings (gray). Paired t-tests, p = 1.44e-5, 0.0276 for the duration of REMs and NREMs episodes.
(F) Frequency of REMs, NREMs, and wake episodes during 6 h of REMs restriction (green) and baseline recordings (gray). Paired t-tests, p = 0.0027 and 0.0043 for the frequency of REMs and NREMs episodes.
(G) Power spectral density (PSD) of EEG during REMs, NREMs, and wakefulness during 6 h of REMs restriction (green) and baseline recordings (gray). Paired t-tests, p = 0.0293 for REMs δ power.
(H) Percentage of time spent in REMs, NREMs, and wakefulness during 1 h of REMs rebound (green, ZT 6.5-7.5) and baseline sleep (gray, ZT 6.5-7.5). Paired t-tests, p = 0.0226 for REMs amount.
(I) Duration of REMs, NREMs, and wake episodes during 1 h of REMs rebound (green) and baseline recordings (gray).
(J) Frequency of REMs, NREMs, and wake episodes during 1 h of REMs rebound (green) and baseline recordings (gray). Paired t-tests, p = 0.0055 for the frequency of REMs episodes.
(K) PSD of EEG during REMs, NREMs, and wakefulness during 1 h of REMs rebound (green) and baseline recordings (gray). Paired t-tests, p = 0.0164 for wake δ power.
(D-F, H-J) Bars, averages across mice; lines, individual mice; error bars, ± s.e.m. n = 10 mice
(G, K) Shadings, ± s.e.m. n = 10 mice in G; n = 9 mice in K, 1 mouse was excluded for REMs because there was no REMs during baseline recordings

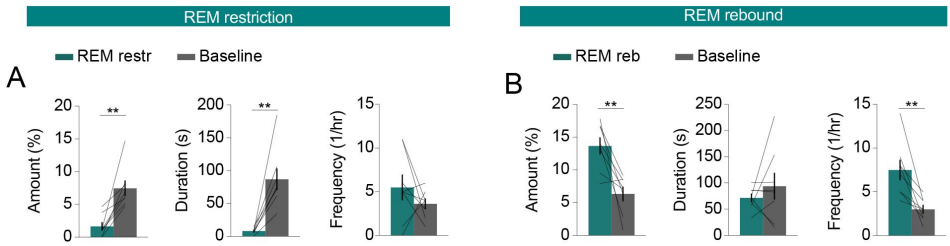

FIGURE S5.

REMs amount, duration, and frequency of episodes during photomery recordings combined with REMs restriction and rebound. Related to Figure 3.

(A) Percentage of REMs, duration, and frequency of REMs episodes during REMs restriction (green, ZT 6.5-7.5) and baseline recordings (gray, ZT 6.5-7.5). Paired t-tests, p = 0.0024, 0.0013 for amount, and duration.
(B) Percentage of REMs, duration, and frequency of REMs episodes during REMs rebound (green, ZT 7.5-8.5) and baseline recordings (gray, ZT 7.5-8.5). Paired t-tests, p = 0.0066, 0.0047 for amount and frequency.
Bars, averages across mice; lines, individual mice; error bars, ± s.e.m.
n = 8 mice

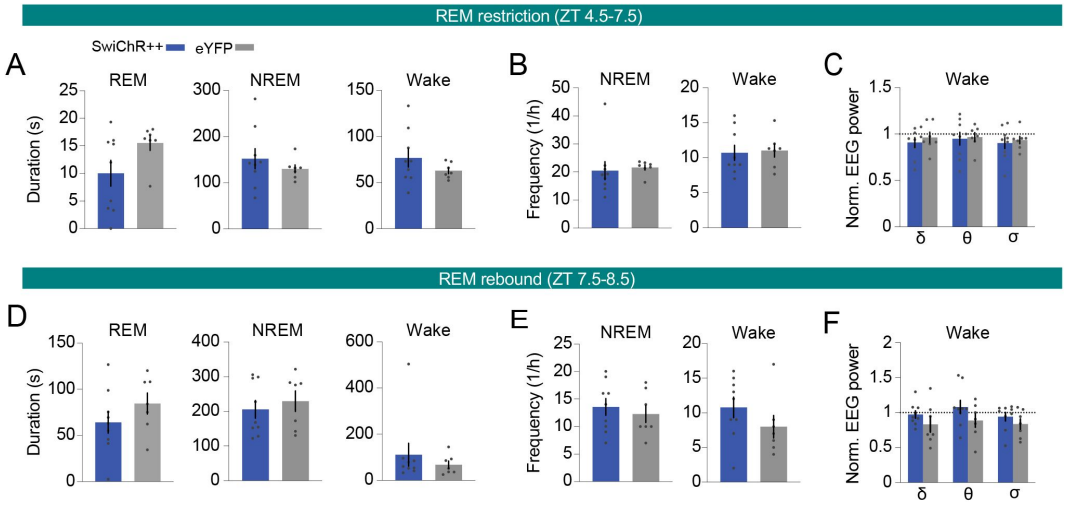

FIGURE S6.

Duration and frequency of REMs episodes and EEG power during SwiChR++-mediated inhibition combined with REMs restriction and rebound. Related to Figure 4.

(A) Duration of REMs, NREMs, and wake episodes during the last 3 h of REMs restriction with laser stimulation (ZT 4.5-7.5) in mice expressing SwiChR++ and eYFP.
(B) Frequency of REMs, NREMs, and wake episodes during the last 3 h of REMs restriction with laser stimulation in mice expressing SwiChR++ and eYFP.
(C) Normalized EEG δ, θ, and σ power during the last 3 h of REMs restriction with laser stimulation in eYFP and SwiChR++ mice.
(D) Duration of REMs, NREMs, and wake episodes during REMs rebound (ZT 7.5-8.5) in mice expressing SwiChR++ and eYFP.
(E) Frequency of REMs, NREMs, and wake episodes during REMs rebound (ZT 7.5-8.5) in mice expressing SwiChR++ and eYFP.
(F) Normalized EEG δ, θ, and σ power during REMs rebound in eYFP and SwiChR++ mice.
Bars, averages across mice; dots, individual mice; error bars, ± s.e.m.
SwiChR++: n = 9 mice; eYFP: n = 7 mice

Figure 1C - ΔF/F (%)						
One-way RM ANOVA		**F**	**DOF**	**p**	**ηp2**	**Sample size**
Main effect of brain state		19.17	(2,18)	0.0009	0.6805	n=10 mice; 24 recordings
Bonferroni's multiple comparisons test	**Comparisons**	**Mean Diff.**	**CI (%)**	**p (adj.)**	**T**	
	REM – Wake	9.774	(3.17, 16.38)	0.0056	4.341	
	REM – NREM	11.48	(4.147, 18.82)	0.0039	4.592	
	Wake – NREM	1.708	(-0.7317, 4.148)	0.2106	2.054	
Figure 1C - ΔF/F (z-scored)						
One-way RM ANOVA		**F**	**DOF**	**p**	**ηp2**	
Main effect of brain state		96.76	(2,18)	2.00E-06	0.9149	
Bonferroni's multiple comparisons test	**Comparisons**	**Mean Diff.**	**CI (%)**	**p (adj.)**	**T**	
	REM – Wake	2.717	(1.731, 3.703)	6.00E-05	8.081	
	REM – NREM	3.072	(2.54, 3.604)	1.00E-07	16.95	
	Wake – NREM	0.3551	(-0.1466, 0.8568)	0.203	2.076	
Figure 1D - ΔF/F NREMs to REMs (z-scored)						
One-way RM ANOVA		**F**	**DOF**	**p**	**ηp2**	**Sample size**
Main effect of time		248.1492	(8,72)	3.18E-49	0.8695	n=10 mice; 24 recordings
Holm-Bonferroni correction Baseline: -60 to -50s	**Comparisons**	**p (adj.)**	**T**	**BF10**	**Hedges' g**	
	Baseline – -50 to -40 s	0.9382	-0.7558	0.392	-0.1073	
	Baseline – -40 to -30 s	0.0419	-3.0426	4.751	-0.7473	
	Baseline – -30 to -20 s	0.0032	-5.5032	92.255	-1.5715	
	Baseline – -20 to -10 s	0.0001	-8.8099	2041.41	-2.7052	
	Baseline – -10 to -0s	1.38E-05	-12.0058	19410	-3.6414	
	Baseline – 0 to 10 s	4.06E-08	-25.0662	5660000	-6.733	
	Baseline – 10 to 20 s	4.06E-08	-25.0011	5545000	-7.3889	
	Baseline – 20 to 30s	4.40E-08	-24.6629	4982000	-6.7371	
Figure 1D - ΔF/F NREMs to wake						
One-way RM ANOVA		**F**	**DOF**	**p**	**ηp2**	**Sample size**
Main effect of time		8.1168	(8,72)	9.50E-08	0.4468	n=10 mice; 24 recordings
Holm-Bonferroni correction Baseline: -60 to -50s	**Comparisons**	**p (adj.)**	**T**	**BF10**	**Hedges' g**	
	Baseline – -50 to -40 s	1.0000	0.135	0.311	0.0389	
	Baseline – -40 to -30 s	1.0000	-0.4897	0.342	-0.1532	
	Baseline – -30 to -20 s	0.7045	-2.3398	1.941	-0.7912	
	Baseline – -20 to -10 s	0.5552	-2.5221	2.441	-0.852	
	Baseline – -10 to -0s	0.0093	-5.707	114.97	-2.0572	
	Baseline – 0 to 10 s	0.0106	-5.5549	97.59	-2.6474	
	Baseline – 10 to 20 s	0.0993	-3.8393	13.089	-1.7162	
	Baseline – 20 to 30s	1.0000	-1.7502	0.961	-0.7732	
Figure 1E - ΔF/F during NREMs						
Paired t tests		**Time**		**p**	**p (adj.)**	**Sample size**
Bonferroni's correction Baseline: 0 to 20%		20 - 40%		2.04E-09	8.14E-09	10 mice; 24 recordings; n=566 events
		40 - 60%		1.66E-12	6.63E-12	
		60 - 80%		1.00E-13	4.01E-13	
		80 - 100%		1.34E-38	5.36E-38	
Figure 2C - REMs amount						
Mixed-effects ANOVA		**F**	**DOF**	**p**	**ηp2**	**Sample size**
Main effect of virus		3.902	(1,19)	0.0629	0.1041	n=12 SwiChR++; n=9 eYFP; 63 recordings
Main effect of laser		18.87	(1,19)	0.0003	0.1755	
Laser x virus		9.388	(1,19)	0.0064	0.3163	
Bonferroni's multiple comparisons test	**Comparisons**	**Mean Diff.**	**CI (%)**	**p (adj.)**	**T**	
	SwiChR++: With laser – W/o laser	-2.119	(-3.031, -1.208)	3.00E-05	5.658	
	eYFP: With laser – W/o laser	-0.3661	(-1.419, 0.6865)	0.8158	0.8463	
	With laser: SwiChR++ – eYFP	-1.941	(-3.365, -0.5173)	0.0058	3.182	
	W/o laser: SwiChR++ – eYFP	-0.1878	(-1.611, 1.236)	1.0000	0.3078	
Figure 2C - NREMs amount						
Mixed-effects ANOVA		**F**	**DOF**	**p**	**ηp2**	
Main effect of virus		1.804	(1,19)	0.195	0.0659	
Main effect of laser		1.266	(1,19)	0.2746	0.0166	
Laser x virus		0.1629	(1,19)	0.691	0.003	
Figure 2C - Wake amount						
Mixed-effects ANOVA		**F**	**DOF**	**p**	**ηp2**	
Main effect of virus		2.153	(1,19)	0.1586	0.0768	
Main effect of laser		2.906	(1,19)	0.1046	0.0361	
Laser x virus		0.6689	(1,19)	0.4236	0.0241	
Figure 2D						
Unpaired t tests		**Mean Diff.**	**CI (%)**	**p**	**T**	
δ: SwiChR++ – eYFP		-0.1107	(-0.218, -0.0034)	0.0432	2.166	
θ: SwiChR++ – eYFP		-0.0845	(-0.1917, 0.0228)	0.1156	1.649	
σ: SwiChR++ – eYFP		-0.1299	(-0.2248, -0.035)	0.0099	2.865	
Figure 2E						
Unpaired t tests		**Mean Diff.**	**CI (%)**	**p**	**T**	
REMs: SwiChR++ – eYFP		-0.9582	(-2.560, 0.6436)	0.2258	1.252	
NREMs: SwiChR++ – eYFP		0.6776	(-3.191, 4.547)	0.7180	0.3666	

Table S1.

Statistical analysis

Wake: SwiChR++ – eYFP		0.5323	(-4.185, 5.250)	0.8158	0.2362	
Figure 3C - Total number of Ca2+ peaks						
Two-way RM ANOVA		**F**	**DOF**	**p**	**ηp2**	**Sample size**
Main effect of time		4.958	(1,7)	0.0613	0.0349	n=8 mice; 16 recordings
Main effect of treatment		19.56	(1,7)	0.0031	0.1611	
Time x treatment		9.229	(1,7)	0.0189	0.0508	
Bonferroni's multiple comparisons test	**Comparisons**	**Mean Diff.**	**CI (%)**	**p (adj.)**	**T**	
	Restr – Baseline (ZT6.5-7.5)	14.25	(5.576. 22.92)	0.0033	5.973	
	Restr – Reb	9.375	(0.7007, 18.05)	0.0341	3.93	
	Restr – Baseline (ZT7.5-8.5)	13.38	(4.701, 22.05)	0.0049	5.606	
	Baseline (ZT6.5-7.5) – Reb	-4.875	(-13.55, 3.799)	0.4819	2.043	
	Baseline (ZT6.5-7.5) – Baseline (ZT7.5-8.5)	-0.875	(-9.549. 7.799)	1.0000	0.3668	
	Reb – Baseline (ZT7.5-8.5)	4	(-4.674, 12.67)	0.8251	1.677	
Figure 3C - Number of NREM Ca2+ peaks						
Two-way RM ANOVA		**F**	**DOF**	**p**	**ηp2**	**Sample size**
Main effect of time		6.674	(1,7)	0.0363	0.0867	n=8 mice; 16 recordings
Main effect of treatment		8.358	(1,7)	0.0233	0.0738	
Time x treatment		19.76	(1,7)	0.003	0.136	
Bonferroni's multiple comparisons test	**Comparisons**	**Mean Diff.**	**CI (%)**	**p (adj.)**	**T**	
	Restr – Baseline (ZT6.5-7.5)	14	(4.674, 23.33)	0.0057	5.458	
	Restr – Reb	14.5	(5.174, 23.83)	0.0046	5.653	
	Restr – Baseline (ZT7.5-8.5)	12.38	(3.049. 21.70)	0.0115	4.825	
	Baseline (ZT6.5-7.5) – Reb	0.5	(-8.826, 9.826)	1.000	0.1949	
	Baseline (ZT6.5-7.5) – Baseline (ZT7.5-8.5)	-1.625	(-10.95, 7.701)	1.000	0.6335	
	Reb – Baseline (ZT7.5-8.5)	-2.125	-11.45, 7.201)	1.000	0.8285	
Figure 3C - Number of REM Ca2+ peaks						
Two-way RM ANOVA		**F**	**DOF**	**p**	**ηp2**	**Sample size**
Main effect of time		1.882	(1,7)	0.2124	0.0643	n=8 mice; 16 recordings
Main effect of treatment		19.72	(1,7)	0.003	0.1504	
Time x treatment		4.853	(1,7)	0.0634	0.1177	
Figure 3D						
Unpaired t tests		**Mean Diff.**	**CI (%)**	**p**	**T**	**Sample size**
Restr – Baseline (ZT6.5-7.5)		-0.0274	(-0.0359, -0.0188)	6.30E-10	6.31	n=295 restr; n=196 baseline peaks
Figure 3E						
Unpaired t tests		**Mean Diff.**	**CI (%)**	**p**	**T**	**Sample size**
Restr – Baseline (ZT6.5-7.5)		-0.0424	(-0.0836, -0.0012)	0.0437	2.048	n=44 restr; n=42 baseline peaks
Figure 3F						
Unpaired t tests		**Mean Diff.**	**CI (%)**	**p**	**T**	**Sample size**
Reb– Baseline (ZT7.5-8.5)		-0.0120	(-0.0183, -0.0057)	0.0002	3.744	n=180 reb; n=196 baseline peaks
Figure 3G						
Unpaired t tests		**Mean Diff.**	**CI (%)**	**p**	**T**	**Sample size**
Reb– Baseline (ZT7.5-8.5)		0.0697	(-0.0404, 0.0149)	0.3641	0.9112	n=84 reb; n=36 baseline peaks
Figure 4C						
Unpaired t tests		**Mean Diff.**	**CI (%)**	**p**	**T**	**Sample size**
REM: SwiChR++ – eYFP		2.325	(0.3211, 4.329)	0.026	2.488	n=9 SwiChR++; n=7 eYFP
NREM: SwiChR++ – eYFP		2.996	(-7.312, 13.30)	0.5431	0.6233	
Wake: SwiChR++ – eYFP		-4.17	(-16.04, 7.701)	0.4637	0.7533	
Figure 4D						
Unpaired t tests		**Mean Diff.**	**CI (%)**	**p**	**T**	**Sample size**
SwiChR++ – eYFP		5.487	(-0.7955, 11.77)	0.0821	1.873	n=9 SwiChR++; n=7 eYFP
Figure 4E						
Unpaired t tests		**Mean Diff.**	**CI (%)**	**p**	**T**	**Sample size**
REM: δ SwiChR++ – eYFP		0.3336	(0.0996, 0.5677)	0.0091	3.106	n=8 SwiChR++; n=6 eYFP
REM: θ SwiChR++ – eYFP		0.1065	(-0.0906, 0.3035)	0.2619	1.177	
REM: σ SwiChR++ – eYFP		0.08642	(-0.1404, 0.3132)	0.4226	0.8302	
NREM: δ SwiChR++ – eYFP		0.0800	(-0.0712, 0.2313)	0.2736	1.1430	n=9 SwiChR++; n=6 eYFP
NREM: θ SwiChR++ – eYFP		0.1614	(0.0150, 0.3078)	0.0332	2.381	
NREM: σ SwiChR++ – eYFP		0.1659	(0.0107, 0.321)	0.038	2.31	
Figure 4F						
Unpaired t tests		**Mean Diff.**	**CI (%)**	**p**	**T**	**Sample size**
REM: SwiChR++ – eYFP		5.082	(0.9075, 9.256)	0.0205	2.611	n=9 SwiChR++; n=7 eYFP
NREM: SwiChR++ – eYFP		1.414	(-6.269, 9.097)	0.6989	0.3948	
Wake: SwiChR++ – eYFP		-6.195	(-16.31, 3.918)	0.21	1.314	
Figure 4G						
Unpaired t tests		**Mean Diff.**	**CI (%)**	**p**	**T**	**Sample size**

Table S1. (continued)

SwiChR++ – eYFP		1.238	(-1.923, 4.399)	0.4149	0.8401	n=9 SwiChR++; n=7 eYFP
Figure 4H						
Unpaired t tests		**Mean Diff.**	**CI (%)**	**p**	**T**	**Sample size**
REM: δ SwiChR++ – eYFP		0.1165	(-0.1479, 0.3808)	0.3607	0.9451	n=8 SwiChR++; n=7 eYFP
REM: θ SwiChR++ – eYFP		0.1751	(-0.0419, 0.3922)	0.1073	1.695	
REM: σ SwiChR++ – eYFP		0.0584	(-0.1462, 0.2629)	0.5563	0.5995	
NREM: δ SwiChR++ – eYFP		0.0349	(-0.1593, 0.2290)	0.706	0.3850	n=9 SwiChR++; n=7 eYFP
NREM: θ SwiChR++ – eYFP		0.0806	(-0.1016, 0.2628)	0.3587	0.9489	
NREM: σ SwiChR++ – eYFP		0.07111	(-0.1314, 0.2736)	0.4638	0.7532	
Figure S1C - ΔF/F (%)						
One-way RM ANOVA		**F**	**DOF**	**p**	**ηp2**	**Sample size**
Main effect of brain state		6.517	(2,22)	0.0162	0.372	n=12 mice; 107 recordings
Bonferroni's multiple comparisons test	**Comparisons**	**Mean Diff.**	**CI (%)**	**p (adj.)**	**T**	
	REM – Wake	3.011	(0.4927, 5.530)	0.0187	3.372	
	REM – NREM	3.225	(0.4341, 6.883)	0.0908	2.485	
	Wake – NREM	0.2132	(-1.806, 2.233)	1.00	0.2977	
Figure S1C - ΔF/F (z-scored)						
One-way RM ANOVA		**F**	**DOF**	**p**	**ηp2**	
Main effect of brain state		12.31	(2,22)	0.0029	0.5281	
Bonferroni's multiple comparisons test	**Comparisons**	**Mean Diff.**	**CI (%)**	**p (adj.)**	**T**	
	REM – Wake	1.197	(0.4864, 1.908)	0.0018	4.75	
	REM – NREM	1.249	(0.1691, 2.329)	0.0227	3.262	
	Wake – NREM	0.05196	(-0.4622, 0.5662)	1.00	0.285	
Figure S1D - ΔF/F NREMs to REMs (z-scored)						
One-way RM ANOVA		**F**	**DOF**	**p**	**ηp2**	**Sample size**
Main effect of time		7.160	(8, 136)	6.89E-08	0.2254	n=12 mice; 107 recordings
Holm-Bonferroni correction Baseline: -60 to -50s	**Comparisons**	**p (adj.)**	**T**	**BF10**	**Hedges' g**	
	Baseline – -50 to -40 s	0.9687	-1.6228	0.732	-0.2863	
	Baseline – -40 to -30 s	0.3266	-2.5938	3.13	-0.6534	
	Baseline – -30 to -20 s	0.0149	-3.9141	33.98	-1.1513	
	Baseline – -20 to -10 s	0.0067	-4.4643	95.561	-1.5424	
	Baseline – -10 to -0s	0.0994	-4.0978	47.973	-1.5385	
	Baseline – 0 to 10 s	0.0002	-3.8919	32.594	-1.4571	
	Baseline – 10 to 20 s	0.0516	-3.0664	7.124	-1.1493	
	Baseline – 20 to 30s	0.0361	-2.2091	1.679	-0.7868	
Figure S1D - ΔF/F NREMs to wake (z-scored)						
One-way RM ANOVA		**F**	**DOF**	**p**	**ηp2**	**Sample size**
Main effect of time		9.9795	(8, 136)	7.15E-11	0.3137	n=12 mice; 107 recordings
Holm-Bonferroni correction Baseline: -60 to -50s	**Comparisons**	**p (adj.)**	**T**	**BF10**	**Hedges' g**	
	Baseline – -50 to -40 s	1.0000	0.0929	0.244	0.0109	
	Baseline – -40 to -30 s	1.0000	-1.0101	0.38	-0.1782	
	Baseline – -30 to -20 s	0.3133	-2.7081	3.8	-0.5109	
	Baseline – -20 to -10 s	0.1752	-3.0835	7.346	-0.6129	
	Baseline – -10 to -0s	0.8944	-1.7431	0.855	-0.4372	
	Baseline – 0 to 10 s	0.0050	4.8473	195.709	1.7266	
	Baseline – 10 to 20 s	0.6455	2.0935	1.408	0.7209	
	Baseline – 20 to 30s	0.5446	2.2762	1.865	0.7958	
Figure S1D - ΔF/F REMs to wake (z-scored)						
One-way RM ANOVA		**F**	**DOF**	**p**	**ηp2**	**Sample size**
Main effect of time		39.1134	(8, 136)	1.07E-31	0.3293	n=12 mice; 107 recordings
Holm-Bonferroni correction Baseline: -60 to -50s	**Comparisons**	**p (adj.)**	**T**	**BF10**	**Hedges' g**	
	Baseline – -50 to -40 s	0.5099	-2.1932	1.638	-0.1471	
	Baseline – -40 to -30 s	0.0730	-3.2648	10.196	-0.3094	
	Baseline – -30 to -20 s	0.4171	-2.3346	2.046	-0.2224	
	Baseline – -20 to -10 s	0.5099	-2.1842	1.616	-0.2956	
	Baseline – -10 to -0s	0.5930	-2.0212	1.264	-0.3061	
	Baseline – 0 to 10 s	1.99E-06	7.0400	9547.365	1.0485	
	Baseline – 10 to 20 s	2.06E-08	9.8071	629000	2.0176	
	Baseline – 20 to 30s	8.33E-07	7.5238	21070	1.7406	
Figure S1D - ΔF/Fwake to NREMs (z-scored)						
One-way RM ANOVA		**F**	**DOF**	**p**	**ηp2**	**Sample size**
Main effect of time		13.17495741	(8, 136)	5.71E-14	0.2193	n=12 mice; 107 recordings
Holm-Bonferroni correction Baseline: -60 to -50s	**Comparisons**	**p (adj.)**	**T**	**BF10**	**Hedges' g**	
	Baseline – -50 to -40 s	1.0000	0.9997	0.376	0.0596	
	Baseline – -40 to -30 s	1.0000	1.5243	0.648	0.1070	
	Baseline – -30 to -20 s	0.4493	2.2974	1.928	0.2584	
	Baseline – -20 to -10 s	0.0010	5.5047	656.926	0.6493	
	Baseline – -10 to -0s	9.10E-09	13.1201	36970000	1.5180	
	Baseline – 0 to 10 s	0.0001	7.1061	10650	1.7551	
	Baseline – 10 to 20 s	0.0054	4.6368	132.06	1.3416	
	Baseline – 20 to 30s	0.2818	2.6283	3.318	0.9186	
Figure S2C - ΔF/F (%)						
One-way RM ANOVA		**F**	**DOF**	**p**	**ηp2**	**Sample size**
Main effect of brain state		19.68	(2,20)	5.23E-04	0.6631	

Table S1. (continued)

Bonferroni's multiple comparisons test	**Comparisons**	**Mean Diff.**	**CI (%)**	**p (adj.)**	**T**	n=11 mice; 41 recordings
	REM – Wake	-3.557	(-5.835, -1.28)	0.0035	4.482	
	REM – NREM	-0.3531	(-1.222, 0.516)	0.8121	1.166	
	Wake – NREM	3.204	(1.280, 5.129)	0.0022	4.779	
Figure S2C - ΔF/F (z-scored)						
One-way RM ANOVA		**F**	**DOF**	**p**	**ηp2**	
Main effect of brain state		147.2	(2,20)	1.862E-11	0.9364	
Bonferroni's multiple comparisons test	**Comparisons**	**Mean Diff.**	**CI (%)**	**p (adj.)**	**T**	
	REM – Wake	-1.514	(-1.837, -1.192)	2.95E-07	13.46	
	REM – NREM	-0.1439	(-0.4172, 0.1295)	0.49	1.511	
	Wake – NREM	1.37	(1.134, 1.607)	3.81E-08	16.66	
Figure S2D - ΔF/F NREMs to REMs (z-scored)						
One-way RM ANOVA		**F**	**DOF**	**p**	**ηp2**	**Sample size**
Main effect of time		14.1919	(8,80)	1.18E-12	0.4003	
Holm-Bonferroni correction Baseline: -60 to -50s	**Comparisons**	**p (adj.)**	**T**	**BF10**	**Hedges' g**	n=11 mice; 41 recordings
	Baseline – -50 to -40 s	1.0000	1.3200	0.597	0.3013	
	Baseline – -40 to -30 s	0.8771	2.0335	1.334	0.4797	
	Baseline – -30 to -20 s	0.7413	2.3087	1.895	0.5665	
	Baseline – -20 to -10 s	1.0000	1.5964	0.797	0.3430	
	Baseline – -10 to -0s	1.0000	0.0139	0.298	0.0034	
	Baseline – 0 to 10 s	1.0000	-1.3712	0.628	-0.5128	
	Baseline – 10 to 20 s	0.3201	-2.9223	4.316	-1.1692	
	Baseline – 20 to 30s	0.1247	-3.5060	9.596	-1.5181	
Figure S2D - ΔF/F NREMs to wake (z-scored)						
One-way RM ANOVA		**F**	**DOF**	**p**	**ηp2**	**Sample size**
Main effect of time		111.2735	(8,80)	4.28E-40	0.8335	
Holm-Bonferroni correction Baseline: -60 to -50s	**Comparisons**	**p (adj.)**	**T**	**BF10**	**Hedges' g**	n=11 mice; 41 recordings
	Baseline – -50 to -40 s	1.0000	1.1771	0.523	0.1151	
	Baseline – -40 to -30 s	0.1716	3.0063	4.841	0.4314	
	Baseline – -30 to -20 s	0.0643	3.7499	13.37	0.5532	
	Baseline – -20 to -10 s	0.5568	2.2209	1.692	0.4427	
	Baseline – -10 to -0s	0.2252	2.8008	3.658	0.3629	
	Baseline – 0 to 10 s	1.41E-05	-11.3691	30510	-3.1566	
	Baseline – 10 to 20 s	1.35E-05	-11.6411	37120	-4.1001	
	Baseline – 20 to 30s	1.44E-05	-11.1641	26250	-4.0837	
Figure S2D - ΔF/F REMs to wake (z-scored)						
One-way RM ANOVA		**F**	**DOF**	**p**	**ηp2**	**Sample size**
Main effect of time		32.6242	(8,80)	3.69E-22	0.5089	
Holm-Bonferroni correction Baseline: -60 to -50s	**Comparisons**	**p (adj.)**	**T**	**BF10**	**Hedges' g**	n=11 mice; 41 recordings
	Baseline – -50 to -40 s	1.0000	0.1931	0.302	0.0203	
	Baseline – -40 to -30 s	1.0000	-1.4257	0.664	-0.1436	
	Baseline – -30 to -20 s	0.6239	-2.3364	1.965	-0.2845	
	Baseline – -20 to -10 s	1.0000	-1.5107	0.726	-0.2829	
	Baseline – -10 to -0s	1.0000	-1.0521	0.469	-0.1834	
	Baseline – 0 to 10 s	0.0008	-7.4133	1034.434	-2.6524	
	Baseline – 10 to 20 s	0.0020	-6.5109	401.011	-2.0901	
	Baseline – 20 to 30s	0.0524	-3.9765	18.141	-1.2891	
Figure S2D - ΔF/F Wake to NREM (z-scored)						
One-way RM ANOVA		**F**	**DOF**	**p**	**ηp2**	**Sample size**
Main effect of time		35.7154	(8,80)	2.38E-23	0.4886	
Holm-Bonferroni correction Baseline: -60 to -50s	**Comparisons**	**p (adj.)**	**T**	**BF10**	**Hedges' g**	n=11 mice; 41 recordings
	Baseline – -50 to -40 s	0.0722	-3.5187	9.763	-0.5254	
	Baseline – -40 to -30 s	0.0743	-3.4133	8.455	-0.8971	
	Baseline – -30 to -20 s	0.0087	-5.1053	77.953	-1.4173	
	Baseline – -20 to -10 s	0.0099	-4.9858	67.18	-1.5718	
	Baseline – -10 to -0s	0.3056	-2.3862	2.098	-0.8628	
	Baseline – 0 to 10 s	9.36E-02	3.2084	6.386	1.0398	
	Baseline – 10 to 20 s	7.43E-02	3.4531	8.928	1.1135	
	Baseline – 20 to 30s	3.46E-02	4.0542	20.125	1.1242	
Figure S2E - ΔF/F during NREMs						
Paired t tests		**Time**		**p**	**p (adj.)**	**Sample size**
Bonferroni's correction Baseline: 0 to 20%		20 - 40%		1.34E-33	5.36E-33	11 mice; 41 recordings; n=889 events
		40 - 60%		3.11E-46	1.24E-45	
		60 - 80%		4.38E-61	1.75E-60	
		80 - 100%		6.48E-71	2.59E-70	
Figure S3A - REM duration						
Mixed-effects ANOVA		**F**	**DOF**	**p**	**ηp2**	**Sample size**
Main effect of virus		0.2531	(1,19)	0.6207	0.0084	
Main effect of laser		0.0040	(1,19)	0.9501	0.0005	
Laser x virus		2.629	(1,19)	0.1214	0.0831	
Figure S3A - NREM duration						
Mixed-effects ANOVA		**F**	**DOF**	**p**	**ηp2**	
Main effect of virus		10.34	(1,19)	0.0046	0.2803	
Main effect of laser		0.3348	(1,19)	0.5697	0.0038	
Laser x virus		0.0081	(1,19)	0.929	0.0002	

Table S1. (continued)

Figure S3A - Wake duration					
Mixed-effects ANOVA	**F**	**DOF**	**p**	**ηp2**	
Main effect of virus	0.192	(1,19)	0.6662	0.0070	
Main effect of laser	2.982	(1,19)	0.1004	0.0455	
Laser x virus	2.399	(1,19)	0.1379	0.0424	n=12 SwiChR++; n=9 eYFP; 63 recordings
Figure S3B - REM frequency					
Mixed-effects ANOVA	**F**	**DOF**	**p**	**ηp2**	
Main effect of virus	2.901	(1,19)	0.1048	0.0712	
Main effect of laser	3.863	(1,19)	0.0642	0.0858	
Laser x virus	1.285	(1,19)	0.2711	0.0604	
Figure S3B - NREM frequency					
Mixed-effects ANOVA	**F**	**DOF**	**p**	**ηp2**	
Main effect of virus	3.715	(1,19)	0.069	0.135	
Main effect of laser	0.0762	(1,19)	0.7854	0.001	
Laser x virus	0.0655	(1,19)	0.8008	0.008	
Figure S3B - Wake frequency					
Mixed-effects ANOVA	**F**	**DOF**	**p**	**ηp2**	
Main effect of virus	9.142	(1,19)	0.007	0.2808	
Main effect of laser	0.0006	(1,19)	0.98	0.0078	
Laser x virus	0.7833	(1,19)	0.7833	0.0002	
Figure S3C - REM EEG power					
Paired t tests	**Mean Diff.**	**CI (%)**	**p**	**T**	**Sample size**
δ: SwiChR++ with laser - w/o laser	-153.7	(-250.1, -57.45)	0.0048	3.514	
θ: SwiChR++ with laser - w/o laser	-198	(-431.7, 35.78)	0.0892	1.864	
σ: SwiChR++ with laser - w/o laser	-68.81	(-122, -15.64)	0.0158	2.848	
Figure S3C - NREM EEG power					
Paired t tests	**Mean Diff.**	**CI (%)**	**p**	**T**	
δ: SwiChR++ with laser - w/o laser	-174.8	(-1036, 686.2)	0.6636	0.4469	
θ: SwiChR++ with laser - w/o laser	113.6	(-134.3, 361.5)	0.3348	1.009	n=12 mice; 36 recordings
σ: SwiChR++ with laser - w/o laser	146.5	(-17.02, 309.9)	0.0743	1.972	
Figure S3C - Wake EEG power					
Paired t tests	**Mean Diff.**	**CI (%)**	**p**	**T**	
δ: SwiChR++ with laser - w/o laser	71.88	(-34.13, 177.9)	0.1637	1.492	
θ: SwiChR++ with laser - w/o laser	26.43	(-140.3, 193.1)	0.7337	0.349	
σ: SwiChR++ with laser - w/o laser	16.81	(-18.88, 52.51)	0.3221	1.037	
Figure S3D - Norm. NREM, wake EEG power					
Unpaired t tests	**Mean Diff.**	**CI (%)**	**p**	**T**	**Sample size**
NREM: δ SwiChR++ – eYFP	-0.0300	(-0.1942, 0.1343)	0.7067	0.382	
NREM: θ SwiChR++ – eYFP	0.0365	(-0.0608, 0.1338)	0.4418	0.7856	
NREM: σ SwiChR++ – eYFP	0.0574	(-0.0524, 0.1672)	0.2877	1.094	n=12 SwiChR++; n=9 eYFP; 63 recordings
Wake: δ SwiChR++ – eYFP	0.0094	(-0.0701, 0.0882)	0.8076	0.2469	
Wake: θ SwiChR++ – eYFP	0.0108	(-0.1057, 0.1273)	0.8479	0.1944	
Wake: σ SwiChR++ – eYFP	0.0064	(-0.0604, 0.0732)	0.8423	0.2017	
Figure S3E - Effect of post laser inhibition on brain state duration					
Unpaired t tests	**Mean Diff.**	**CI (%)**	**p**	**T**	**Sample size**
REMs: SwiChR++ – eYFP	-3.906	(-15.73, 7.921)	0.4978	0.6912	n=12 SwiChR++; n=9 eYFP; 63 recordings
NREMs: SwiChR++ – eYFP	18.65	(-15.91, 53.20)	0.2728	1.129	
Wake: SwiChR++ – eYFP	34.67	(-3.241, 72.58)	0.0708	1.914	
Figure S3F - Effect of post laser inhibition on brain state frequency					
Unpaired t tests	**Mean Diff.**	**CI (%)**	**p**	**T**	**Sample size**
REMs: SwiChR++ – eYFP	-0.1972	-(1.594, 1.200)	0.7709	0.2954	n=12 SwiChR++; n=9 eYFP; 63 recordings
NREMs: SwiChR++ – eYFP	-2.04	(-5.713, 1.634)	0.2596	1.162	
Wake: SwiChR++ – eYFP	-0.7592	(-2.521, 1.002)	0.3784	0.902	
Figure S4B - Motor-on frequency					
One-way RM ANOVA	**F**	**DOF**	**p**	**ηp2**	**Sample size**
Main effect of time	5.835	(5,45)	0.0061	0.3933	
Comparisons	**Mean Diff.**	**CI (%)**	**p (adj.)**	**T**	
Bonferroni's multiple comparisons test Baseline: ZT1.5 — ZT1.5 – ZT2.5	-6.1	(-12.54, 0.3353)	0.0656	3.081	
Bonferroni's multiple comparisons test Baseline: ZT1.5 — ZT1.5 – ZT3.5	-9.1	(-17.46, -0.7447)	0.0316	3.539	n=10 mice; 10 recordings
Bonferroni's multiple comparisons test Baseline: ZT1.5 — ZT1.5 – ZT4.5	-15.8	(-29.76, -1.845)	0.0254	3.679	
Bonferroni's multiple comparisons test Baseline: ZT1.5 — ZT1.5 – ZT5.5	-14.4	(-27.03, -1.765)	0.0245	3.704	
Bonferroni's multiple comparisons test Baseline: ZT1.5 — ZT1.5 – ZT6.5	-16.4	(-27.86, -4.944)	0.006	4.652	
Figure S4D - Effect of REM restriction on brain state amount					
Paired t tests	**Mean Diff.**	**CI (%)**	**p**	**T**	**Sample size**
REMs: Restriction - Baseline	2.748	(1.536, 3.960)	0.0006	5.128	
NREMs: Restriction - Baseline	-7.06	(-16.91, 2.791)	0.1394	1.621	
Wake: Restriction - Baseline	4.631	(-6.168, 15.43)	0.3573	0.9701	
Figure S4E - Effect of REM restriction on brain state duration					
Paired t tests	**Mean Diff.**	**CI (%)**	**p**	**T**	
REMs: Restriction - Baseline	49.16	(35.99, 62.34)	1.44E-05	8.441	
NREMs: Restriction - Baseline	85.41	(11.77, 159.1)	0.0276	2.624	
Wake: Restriction - Baseline	153.00	(-127.4, 433.4)	0.2482	1.235	
Figure S4F - Effect of REM restriction on brain state frequency					
Paired t tests	**Mean Diff.**	**CI (%)**	**p**	**T**	
REMs: Restriction - Baseline	-7.533	(-11.70, -3.370)	0.0027	4.093	
NREMs: Restriction - Baseline	-8.267	(-13.20, -3.336)	0.0043	3.793	n=10 mice; 20 recordings
Wake: Restriction - Baseline	-1.217	(-3.110, 0.6769)	0.18	1.454	
Figure S4G - Effect of REM restriction on power spectral density (PSD)					
Paired t tests	**Mean Diff.**	**CI (%)**	**p**	**T**	
REMs δ: Restriction - Baseline	-160.2	(-300.1, -20.21)	0.0293	2.589	
REMs θ: Restriction - Baseline	-82.12	(-410.1, 245.9)	0.585	0.5664	

Table S1. (continued)

REMs σ: Restriction - Baseline	-90.7	(-190.8, 9.430)	0.0707	2.049	
NREMs δ: Restriction- Baseline	-82.57	(-709.8, 544.7)	0.7726	0.2978	
NREMs θ: Restriction - Baseline	-155.8	(-340.4, 28.85)	0.0887	1.909	
NREMs σ: Restriction - Baseline	-123.4	(-247.3, 0.4201)	0.0506	2.254	
Wake δ: Restriction - Baseline	-193.5	(-457.0, 69.98)	0.131	1.661	
Wake θ: Restriction - Baseline	6.578	(-145.0, 158.1)	0.9239	0.09819	
Wake σ: Restriction - Baseline	-22.51	(-73.01, 27.99)	0.3397	1.008	
Figure S4H - Effect of REM restriction on rebound brain state amount					
Paired t tests	**Mean Diff.**	**CI (%)**	**p**	**T**	**Sample size**
REMs: Rebound - Baseline	-6.444	(-11.75, -1.135)	0.0226	2.746	n=10 mice; 20 recordings
NREMs: Rebound - Baseline	-11.06	(-30.71, 8.583)	0.2346	1.274	
Wake: Rebound - Baseline	17.41	(-7.382,42.20)	0.1466	1.589	
Figure S4I - Effect of REM restriction on rebound brain state duration					
Paired t tests	**Mean Diff.**	**CI (%)**	**p**	**T**	
REMs: Rebound - Baseline	-4.038	(-40.61, 32.54)	0.8084	0.2497	
NREMs: Rebound - Baseline	-3.1	(-7.291, 1.091)	0.1286	1.673	
Wake: Rebound - Baseline	323.7	(-297.6, 945.0)	0.2687	1.179	
Figure S4J - Effect of REM restriction on rebound brain state frequency					
Paired t tests	**Mean Diff.**	**CI (%)**	**p**	**T**	
REMs: Rebound - Baseline	-4.1	(-6.656, -1.544)	0.0055	3.629	
NREMs: Rebound - Baseline	-3.1	(-7.291, 1.091)	0.1286	1.673	
Wake: Rebound - Baseline	-1.217	(-3.110, 0.6769)	0.18	1.454	
Figure S4K - Effect of REM restriction on rebound PSD					
Paired t tests	**Mean Diff.**	**CI (%)**	**p**	**T**	**Sample size**
REMs δ: Rebound - Baseline	-164.5	(-347.5, 18.47)	0.0719	2.073	n=9 mice; 18 recordings
REMs θ: Rebound - Baseline	-178.2	(-540.2, 183.8)	0.2892	1.135	
REMs σ: Rebound - Baseline	-24.13	(-123.5, 75.24)	0.5908	0.56	
NREMs δ: Rebound - Baseline	-96.7	(-897.0, 703.7)	0.7908	0.2733	n=10 mice; 20 recordings
NREMs θ: Rebound - Baseline	-113.8	(-308.6, 81.05)	0.2191	1.321	
NREMs σ: Rebound - Baseline	-55.53	(-231.6, 120.6)	0.4938	0.7132	
Wake δ: Rebound - Baseline	-232.9	(-412.0, -53.88)	0.0164	2.943	
Wake θ: Rebound - Baseline	89.03	(-123.0, 301.1)	0.367	0.9499	
Wake σ: Rebound - Baseline	-24.97	(-108.7, 58.80)	0.5171	0.6742	
Figure S5A - REM restriction for photometry recordings					
Paired t tests	**Mean Diff.**	**CI (%)**	**p**	**T**	**Sample size**
REMs Amount: Restr - Baseline	5.825	(2.839, 8.810)	0.0024	4.614	n=8 mice; 16 recordings
REMs Duration: Restr - Baseline	78.87	(42.61, 115.1)	0.0013	5.143	
REMs Frequency: Restr - Baseline	-1.875	(-5.907, 2.158)	0.3079	1.099	
Figure S5B - Effect of REM restriction on REM rebound for photometry recordings					
Paired t tests	**Mean Diff.**	**CI (%)**	**p**	**T**	**Sample size**
REMs Amount: Reb - Baseline	-7.344	(-11.90, -2.788)	0.0066	3.812	n=8 mice; 16 recordings
REMs Duration: Reb - Baseline	22.6	(-36.03, 81.23)	0.3923	0.9116	
REMs Frequency: Reb - Baseline	-4.5	(-7.105, -1.894)	0.0047	4.084	
Figure S6A - Effect of laser inhibition during REM restriction on brain state duration					
Unpaired t tests	**Mean Diff.**	**CI (%)**	**p**	**T**	**Sample size**
REMs Duration: SwiChR++ - eYFP	5.487	(-0.7955, 11.77)	0.0821	1.873	n=9 SwiChR++; n=7 eYFP
NREMs Duration: SwiChR++ - eYFP	-22.06	(-77.67, 33.55)	0.4092	0.8508	
Wake Duration: SwiChR++ - eYFP	-13.85	(-38.54, 10.84)	0.249	1.203	
Figure S6B - Effect of laser inhibition during REM restriction on brain state frequecy					
Unpaired t tests	**Mean Diff.**	**CI (%)**	**p**	**T**	
NREMs Frequency: SwiChR++ - eYFP	1.138	(-6.909, 9.184)	0.7662	0.3032	
Wake Frequnecy: SwiChR++ - eYFP	0.3439	(-2.823, 3.511)	0.8192	0.2329	
Figure S6C - Effect of laser inhibition during REM restriction on norm. EEG wake					
Unpaired t tests	**Mean Diff.**	**CI (%)**	**p**	**T**	
Wake: δ SwiChR++ – eYFP	0.0704	(-0.1561, 0.2969)	0.5157	0.6669	
Wake: θ SwiChR++ – eYFP	0.0704	(-0.1211, 0.2619)	0.4437	0.7883	
Wake: σ SwiChR++ – eYFP	0.0839	(-0.1104, 0.2780)	0.3701	0.926	
Figure S6D - Effect of laser inhibition during REM restriction on brain state duration					
Unpaired t tests	**Mean Diff.**	**CI (%)**	**p**	**T**	**Sample size**
REMs Duration: SwiChR++ - eYFP	20.16	(-15.75, 56.07)	0.2484	1.204	n=9 SwiChR++; n=7 eYFP
NREMs Duration: SwiChR++ - eYFP	23.57	(-60.14, 107.3)	0.5555	0.604	
Wake Duration: SwiChR++ - eYFP	-43.98	(-169, 81.07)	0.4632	0.7543	
Figure S6E - Effect of laser inhibition during REM restriction on brain state frequecy					
Unpaired t tests	**Mean Diff.**	**CI (%)**	**p**	**T**	
NREMs Frequency: SwiChR++ - eYFP	-1.27	(-5.996, 3.456)	0.5736	0.5763	
Wake Frequnecy: SwiChR++ - eYFP	-2.778	(-7.538, 1.983)	0.2312	1.252	
Figure S6H - Effect of laser inhibition during REM restriction on norm. wake EEG					
Unpaired t tests	**Mean Diff.**	**CI (%)**	**p**	**T**	
Wake: δ SwiChR++ – eYFP	-0.1418	(-0.3875, 0.1039)	0.2362	1.238	
Wake: θ SwiChR++ – eYFP	-0.1937	(-0.4870, 0.0996)	0.1786	1.416	
Wake: σ SwiChR++ – eYFP	-0.1056	(-0.3121, 0.1008)	0.291	1.097	

Table S1. (continued)

Immunohistochemistry

Mice were deeply anesthetized and transcardially perfused with phosphate-buffered saline (PBS) followed by 4% paraformaldehyde (PFA) in PBS. Brains were removed and fixed overnight in 4% PFA in PBS and then stored in 30% sucrose in PBS. Brains were embedded with OCT compound (Tissue-Tek, Sakura Finetek) and frozen. 40 µm sections were cut using a cryostat (Thermo Scientific HM525 NX) and directly mounted onto glass slides. Brain sections were washed in PBS for 5 min, permeabilized using PBST (0.3% Triton X-100 in PBS) for 30 min, and incubated in blocking solution (5% normal donkey serum in 0.3% PBST; 017-000-001, Jackson ImmunoResearch Laboratories) for 1 h. Brain sections were incubated with chicken anti-GFP antibody (1:1,000; GFP8794984, Aves Lab) in the blocking solution overnight at 4°C. The following morning, sections were washed in PBS and incubated for 3 h with the donkey anti-chicken secondary antibody conjugated to a green Alexa fluorophore 488 (1:500; 703-545-155, Jackson ImmunoResearch Laboratories) for 2 h. Afterwards, sections were washed with PBS followed by counterstaining with Hoechst solution (#33342, Thermo Scientific). Slides were coverslipped with mounting medium (Fluoromount-G, Southern Biotechnic) and imaged using a fluorescence microscope (Microscope, Leica DM6B; Camera, Leica DFC7000GT; LED, Leica CTR6 LED) to verify virus expression and optic fiber placement. Animals were excluded if no virus expression is detected or the virus expression/optic fiber tips were not properly localized to the targeted area.

Viral transfection mapping

We generated heatmaps of the virus expression across mice as previously described (Smith et al., 2022; Stucynski et al., 2022; Schott et al., 2023). Coronal reference images for the corresponding AP coordinates were downloaded from the Allen Reference Atlas - Mouse Brain (*atlas.brain-map.org*). For a given AP reference atlas section, the corresponding histology section from each mouse was overlaid and regions in which GCaMP labeled cell bodies were present were manually outlined. Custom Python programs detected these outlines and determined for each location on the reference picture the number of mice with overlapping virus expression, which was encoded using different green color intensities.

Polysomnographic recordings

All sleep recordings were performed in a cage to which the animal had been habituated for several days. All recordings were performed during the light phase between 8 am and 5 pm (ZT1-10) in sound-attenuating chambers. For sleep recordings, EEG and EMG signals were recorded using an RHD2132 amplifier (Intan Technologies, sampling rate 1 kHZ) connected to an RHD USB interface board (Intan Technologies). For fiber photometry experiments, a calcium signal was recorded using an RZ5P amplifier (Tucker-Davis Technologies, sampling rate 1.5 kHz). EEG and EMG signals were referenced to a ground screw located on top of the cerebellum. At the start of each sleep recording, EEG and EMG electrodes were connected to flexible recording cables via small connectors. To determine the brain state of the animal, we first computed the EEG and EMG spectrogram for sliding, half-overlapping 5 s windows, resulting in 2.5 s time resolution. To estimate within each 5 s window the power spectral density (PSD), we performed Welch's method with Hanning window using sliding, half-overlapping 2 s intervals. Next, we computed the time-dependent δ (0.5 to 4 Hz), θ (5 to 12 Hz), σ (12 to 20 Hz), and high γ (100 to 150 Hz) power by integrating the EEG power in the corresponding ranges within the EEG spectrogram. In addition, we calculated the ratio of the θ and δ power (θ/δ) and the EMG power in the range of 50 to 500 Hz. For each power band, we used its temporal mean to separate it into a low and high part (except for the EMG and θ/δ ratio, where we used the mean plus one standard deviation as threshold). REMs was defined by a high θ/δ ratio, low EMG, and low δ power. NREMs was defined by high δ power, a low θ/δ ratio, and low EMG power. In addition, states with low EMG power, low δ power, but high σ power were scored as NREMs. Wake was defined by low δ power, high EMG power and high γ power (if not otherwise classified as REMs). Our automatic algorithm that has been previously used in (Weber et al., 2015, 2018; Chung et al., 2017; Antila et al., 2022; Smith et al., 2022; Stucynski et al., 2022; Schott et al., 2023) has 90.256 % accuracy compared with the

manual scoring by expert annotators. We manually verified the automatic classification using a graphical user interface visualizing the raw EEG and EMG signals, EEG spectrograms, EMG amplitudes, and the hypnogram to correct for errors, by visiting each single 2.5 s epoch in the hypnograms. The software for automatic brain state classification and manual scoring was programmed in Python (*https://github.com/tortugar/Lab/tree/master/PySleep*).

Fiber photometry

Prior to the recording, the optic fiber and EEG/EMG electrodes were connected to flexible patch cables. For calcium imaging, a first LED (Doric lenses) generated the excitation wavelength of 465 nm and a second LED emitted 405 nm light, which served as control for bleaching and motion artifacts. 465 and 405 nm signals were modulated at two different frequencies, 210 and 330 Hz respectively. Both lights traveled through dichroic mirrors (Doric lenses) before entering a patch cable attached to the optic fiber. Fluorescence signals emitted by GCaMP8s or GCaMP6s were collected by the optic fiber and traveled via the patch cable through a dichroic mirror and GFP emission filter (Doric lenses) before entering a photoreceiver (Newport Co.). Photoreceiver signals were relayed to an RZ5P amplifier and demodulated into two signals using the Synapse software (Tucker-Davis Technologies), corresponding to the 465 and 405 nm excitation wavelengths. To analyze the calcium activity, we used custom-written Python scripts. First, both signals were low-pass filtered at 2 Hz using a 4th order digital Butterworth filter. Next, we fitted the 405 nm to the 465 nm signal using linear regression. Finally, the linear fit was subtracted from the 465 nm signal to correct for photobleaching and/or motion artifacts, and the difference was divided by the linear fit yielding the ΔF/F signal. Both the fluorescence signals and EEG/EMG signals were simultaneously recorded using the RZ5P amplifier. Fiber photometry recordings were excluded if the signals suddenly shifted, likely due to a loose connection between the optic fiber and patch cable.

Optogenetic manipulation

Sleep recordings were performed during the light phase (ZT2-8). Mice were tethered to bilateral patch cables connected with the lasers and a flexible recording cable to record EEG/EMG signals. The recording started after 30 min of habituation. For optogenetic inhibition experiments, 2 s step pulses (1-3 mW, 60 s intervals) were generated by a blue laser (473 nm, Laserglow) and sent through the optic fiber (200 um diameter, Thorlabs) connected to the ferrule on the animal's head for 3 h (ZT2-5). TTL pulses to trigger the laser were controlled using a Raspberry Pi, which was controlled by a custom-programmed user interface programmed in Python. Following sustained inhibition, an additional 3 h (ZT5-8) recording was performed without laser stimulation (post-laser session). Baseline recordings were performed (without laser stimulation, ZT2-5), and counterbalanced across mice and days to avoid potential order effects. For each mouse, we collected 2-3 baseline and laser recordings each.

REMs restriction

We employed an automatic REMs detection algorithm (Weber et al., 2015, 2018; Stucynski et al., 2022; Schott et al., 2023) and used a small vibrating motor to terminate/restrict REMs (Cardis et al., 2021; Osorio-Forero et al., 2023) (*https://github.com/luthilab/IntanLuthiLab*). A small vibrating motor (DC 3V Mini Vibration Motor, diameter: 10mm, thickness: 3mm, BOJACK) with a soldered lobster claw clasp was attached to a small wire hook secured in the dental cement of each mouse head. The motors had cables that were connected to a Raspberry Pi which controlled the motor onset and offset.

The automatic REMs detection algorithm determined whether the mouse was in REMs or not based on real-time spectral analysis of the EEG/EMG signals. The onset of REMs was defined as the time point where the EEG θ/δ ratio exceeded a threshold (mean + 1 std of θ/δ), which was calculated from the same mouse using previous recordings. As soon as a REMs episode was

detected, the small vibrating motor turned on to terminate REMs and consequently woke up the mouse. The motor vibrated until the REMs episode was terminated, i.e. when the θ/δ ratio dropped below its mean value or if the EMG amplitude surpassed a threshold (mean + 0.5 std of amplitude). All REMs restriction experiments started at ZT1.5 and lasted until ZT7.5. Following the restriction, motors were turned off and mice were permitted to enter recovery sleep.

To monitor the calcium activity during REMs restriction using fiber photometry, we performed manual REMs restriction to avoid potential motion artifacts caused by the vibrating motor that could interfere with the integrity of the fiber photometry signals. Briefly mice underwent a 4 h automatic REMs restriction protocol as described above. During the last 2 h of restriction, REMs was detected manually based on the EEG and EMG signal by an experimenter who gently pulled on a string attached to the hook secured in the dental cement of the mouse head. To avoid potential photobleaching, the recording was performed during the last 1 h of REMs restriction and 1 h of REMs rebound. Each mouse also underwent a baseline recording on a separate day. The order of REMs restriction and baseline recordings were varied to minimize the impact of the experimental sequence on the results.

We also performed automatic REMs restriction combined with optogenetic inhibition. Each mouse underwent REMs restriction for 6 h, and we continuously delivered 2 s step pulses (1-3 mw, 473 nm, Laserglow) at 60 s intervals during the last 3 h of restriction (ZT4.5-7.5). Following REMs restriction, the recovery sleep was recorded.

Analysis of ΔF/F activity at brain state transitions and during NREMs

To calculate the activity of $POA^{GAD2} \rightarrow TMN$ neurons relative to brain state transitions (**Fig. 1D**), we aligned the ΔF/F signals for transitions across all mice relative to the time point of the transition (t = 0 s). For each NREMs → REMs or NREMs → Wake transition, we ensured that the preceding NREMs episodes lasted for at least 60 s, only interrupted by short awakenings (≤ 20 s). To determine the time point at which the activity significantly started to increase or decrease, we used the first 10 s of NREMs as baseline. For REMs → Wake and Wake → NREMs transitions, the preceding REMs or Wake episode was at least 30 s long. Using one-way rm ANOVA, we tested whether the activity (downsampled to 10s bins) within each 10 s bin was significantly modulated throughout the transition (from -60 to 30 s). Finally, using pairwise t-tests with Holm-Bonferroni correction, we determined the time bins for which the activity significantly differed from the baseline bin (activity for bin -60 to -50 s). The time point for a given 10 s bin was set to its midpoint. To account for multiple comparisons, we divided the significance level (α = 0.05) by the number of comparisons (Bonferroni correction). To analyze the activity throughout NREMs, we normalized the duration of all NREMs episodes and the corresponding ΔF/F signals to the same length.

Spectrotemporal correlation analysis

To identify features of the EEG spectrogram associated with $POA^{GAD2} \rightarrow TMN$ calcium activity, we adapted a receptive field model (Weber et al., 2010; Schott et al., 2023) to predict $POA^{GAD2} \rightarrow TMN$ neural activity from the spectrogram. Intuitively, we estimated a spectrotemporal filter using linear regression that predicts for each time point the $POA^{GAD2} \rightarrow TMN$ calcium response. In more detail, we first computed the EEG spectrogram $E(f_i, t_j)$ using 2 s windows with 80 % overlap, resulting in a time resolution dt of 400 ms. Each spectrogram frequency was normalized by its mean power across the recording, and the parameter $E(f_i, t_j)$ specifies the relative amplitude of frequency f_i for time point t_j. We then downsampled the ΔF/F response using the same time resolution as for the spectrogram, and extracted all time bins with REMs, NREMs or wake for analysis.

To predict the calcium response, the EEG spectrogram was linearly filtered with the kernel $H(f_i, t_l)$. In analogy to receptive fields estimated using similar approaches for sensory neurons, we used the term "spectral field" for $H(f_i, t_l)$. The spectral field can be described as the set of coefficients that optimally relate the neural activity at time t_j to the EEG spectrogram at time t_{j+l}, where l represents the lag between the time points of the spectrogram and the neural response. The estimated frequency components of $H(f_i, t_l)$ ranged from f_1 = 0.5 Hz to f_{nf} = 20 Hz, while the time axis ranged from $-n_T * dt$ = -50 s to $n_T * dt$ = 50 s. Thus, $H(f_i, t_l)$ comprises n_f frequencies and $2 * n_T + 1$ time bins over a window from -50 to +50 seconds relative to the neural response. The convolution of the EEG spectrogram with the spectral field can be expressed as

$$\hat{r}(t_j) = r_0 + \sum_{l=-n_T}^{n_T} \sum_{i=1}^{n_f} E(f_i, t_{j+l})\, H(f_i, t_l) \qquad \text{(Eq. 1)}$$

The scalar parameter r denotes a constant offset, and $\hat{r}(t_j)$ denotes the predicted neural response. The optimal spectral field $H(f_i, t_l)$ minimizes the mean-squared error between the predicted and measured neural response at time t_j. To account for the large number of estimated parameters, we included a regularization term in the error function, which penalizes large kernel components and therefore guards against overfitting of the model. The spectral field for each recording was estimated using 5-fold cross-validation to determine the regularization parameter (λ) that optimized the average model performance on the test sets. Kernels were averaged across all recordings for individual animals; the spectrotemporal correlation in **Fig. 1F** represents the mean spectral field across all mice.

Power spectral density and power estimation

The power spectral density (PSD) of the EEG was computed using Welch's method with the Hanning window for sliding, half-overlapping 2 s intervals. To calculate the power within a given frequency band, we approximated the corresponding area under the spectral density curve using a midpoint Riemann sum. To compute the EMG amplitude, we calculated the PSD of the EMG and integrated frequencies between 5 - 100 Hz. To test whether laser stimulation changed the spectral density during a specific brain state, we determined for each mouse the δ, θ or σ power for that state with and without laster. To compare the PSD between experimental and control mice, we calculated the δ, θ, and σ power with and without laser stimulation for each mouse and normalized the power values with laser by the power obtained for epochs without laser.

Detection of calcium transients

To detect calcium transients, we first filtered the ΔF/F signal with a zero-lag, 4th order digital Butterworth filter with cutoff frequency of 1/20 Hz. Next, prominent peaks in the signal were detected using the function scipy.find_peaks provided by the open source Python library scipy (*https://scipy.org*). As parameter for the peak prominence, we used 0.15 * distance between the 1st and 99th percentile of the distribution of the ΔF/F signal. A transient was defined as occurring during NREMs and REMs, if the peak overlapped with NREMs or REMs respectively. The calcium transient amplitude was calculated by using the values 10 s preceding the peak and subtracting that from the peak values at 0 s.

Statistical tests

Statistical analyses were performed using the python modules (scipy.stats, *https://scipy.org*; pingouin, *https://pingouin-stats.org*) and Prism v9.5.0.0 (GraphPad Software Inc). We did not predetermine sample sizes, but cohorts were similarly sized as in other relevant sleep studies (Jego et al., 2013; Ma et al., 2019). All data collection was randomized and counterbalanced. All data are reported as mean ± s.e.m. A (corrected) p-value < 0.05 was considered statistically significant for all comparisons. Data were compared using unpaired *t*-tests, paired *t*-tests, one-way ANOVAs, or two-way ANOVAs followed by multiple comparisons as appropriate. The statistical results for the figures are presented in the **Table S1**, and Figure legends.

Data sharing plans

The code used for data analysis is publicly available under: *https://github.com/tortugar/Lab*. All the data are available from the corresponding author upon reasonable request.

Acknowledgements

We thank Mandy Schott for generating python scripts for optogenetic manipulation during REMs restriction, Jenny Smith for help with generating the virus expression heatmaps and members of the Chung and Weber labs for helpful discussion. This work was funded by the National Institute of Neurological Disorders and Stroke (R01-NS-110865), the Whitehall Foundation, the Alfred P. Sloan Foundation, a NARSAD Young Investigator Grant from the Brain & Behavior Research Foundation, a Simons Foundation Pilot Award, an Eagle Autism Challenge Pilot Grant, the Thomas B. and Jeannette E. Laws McCabe Fund Award, the Hartwell Individual Biomedical Research Award (to S.C.), and the NIH individual F31 fellowship (NS118963-01A1, to J.M).

Author contributions

Conceptualization: J.M., F.W., and S.C.; Methodology: J.M., X.J., J.H., R.C., A.O-F. A.Lüthi, F.W., and S.C.; Software: J.M., X.J., and F.W.; Validation: J.M., A.Lin, and N.S.; Formal Analysis: J.M.; Investigation: J.M. and A.Lin; Resources: J.M., F.W., and S.C.; Data Curation: J.M. and A.Lin; Writing –Original Draft: J.M.; Writing –Review and Editing: J.M., R.C., A.O-F. A.Lüthi, F.W., and S.C.; Visualization: J.M.; Supervision: S.C.; Funding Acquisition: J.M. and S.C.

References

Antila H., Kwak I., Choi A., Pisciotti A., Covarrubias I., Baik J., et al. (2022) **A noradrenergic-hypothalamic neural substrate for stress-induced sleep disturbances** *Proc. Natl. Acad. Sci. U. S. A* **119** https://doi.org/10.1073/pnas.2123528119

Bayliss D. A., Wang Y. M., Zahnow C. A., Joseph D. R., Millhorn D. E (1990) **Localization of histidine decarboxylase mRNA in rat brain** *Mol. Cell. Neurosci* **1**:3–9 https://doi.org/10.1016/1044-7431(90)90036-4

Beersma D. G., Dijk D. J., Blok C. G., Everhardus I (1990) **REM sleep deprivation during 5 hours leads to an immediate REM sleep rebound and to suppression of non-REM sleep intensity** *Electroencephalogr. Clin. Neurophysiol* **76**:114–122 https://doi.org/10.1016/0013-4694(90)90209-3

Benington J. H., Woudenberg M. C., Heller H. C (1994) **REM-sleep propensity accumulates during 2-h REM-sleep deprivation in the rest period in rats** *Neurosci. Lett* **180**:76–80 https://doi.org/10.1016/0304-3940(94)90917-2

Berndt A., Lee S. Y., Wietek J., Ramakrishnan C., Steinberg E. E., Rashid A. J., et al. (2016) **Structural foundations of optogenetics: Determinants of channelrhodopsin ion selectivity** *Proc. Natl. Acad. Sci. U. S. A* **113**:822–829 https://doi.org/10.1073/pnas.1523341113

Cardis R., Lecci S., Fernandez L. M., Osorio-Forero A., Chung Chu Sin, Fulda P., et al. (2021) **Cortico-autonomic local arousals and heightened somatosensory arousability during NREMS of mice in neuropathic pain** *eLife* **10** https://doi.org/10.7554/eLife.65835

Chung S., Weber F., Zhong P., Tan C. L., Nguyen T. N., Beier K. T., et al. (2017) **Identification of preoptic sleep neurons using retrograde labelling and gene profiling** *Nature* **545**:477–481 https://doi.org/10.1038/nature22350

Clément O., Sapin E., Bérod A., Fort P., Luppi P.-H (2011) **Evidence that neurons of the sublaterodorsal tegmental nucleus triggering paradoxical (REM) sleep are glutamatergic** *Sleep* **34**:419–423 https://doi.org/10.1093/sleep/34.4.419

Donlea J. M., Pimentel D., Miesenböck G (2014) **Neuronal Machinery of Sleep Homeostasis in Drosophila** *Neuron* **81**:860–872 https://doi.org/10.1016/j.neuron.2013.12.013

Endo T., Schwierin B., Borbély A. A., Tobler I (1997) **Selective and total sleep deprivation: effect on the sleep EEG in the rat** *Psychiatry Res* **66**:97–110 https://doi.org/10.1016/s0165-1781(96)03029-6

Endo T., Roth C., Landolt H. P., Werth E., Aeschbach D., Achermann P., et al. (1998) **Selective REM sleep deprivation in humans: effects on sleep and sleep EEG** *Am. J. Physiol* **274**:R1186–1194 https://doi.org/10.1152/ajpregu.1998.274.4.R1186

Franken P (2002) **Long-term vs. short-term processes regulating REM sleep** *J. Sleep Res* **11**:17–28 https://doi.org/10.1046/j.1365-2869.2002.00275.x

Germain A (2013) **Sleep disturbances as the hallmark of PTSD: where are we now?** *Am. J. Psychiatry* **170**:372–382 https://doi.org/10.1176/appi.ajp.2012.12040432

Gong H., McGinty D., Guzman-Marin R., Chew K.-T., Stewart D., Szymusiak R (2004) **Activation of c-fos in GABAergic neurones in the preoptic area during sleep and in response to sleep deprivation** *J. Physiol* **556**:935–946 https://doi.org/10.1113/jphysiol.2003.056622

Gottesmann C (1996) **The transition from slow-wave sleep to paradoxical sleep: evolving facts and concepts of the neurophysiological processes underlying the intermediate stage of sleep** *Neurosci. Biobehav. Rev* **20**:367–387 https://doi.org/10.1016/0149-7634(95)00055-0

Gottesmann C., Gottesman I (2007) **The neurobiological characteristics of rapid eye movement (REM) sleep are candidate endophenotypes of depression, schizophrenia, mental retardation and dementia** *Prog. Neurobiol* **81**:237–250 https://doi.org/10.1016/j.pneurobio.2007.01.004

Gvilia I., Turner A., McGinty D., Szymusiak R (2006) **Preoptic Area Neurons and the Homeostatic Regulation of Rapid Eye Movement Sleep** *J. Neurosci* **26**:3037–3044 https://doi.org/10.1523/JNEUROSCI.4827-05.2006

Haas H. L., Sergeeva O. A., Selbach O (2008) **Histamine in the Nervous System** *Physiol. Rev* **88**:1183–1241 https://doi.org/10.1152/physrev.00043.2007

Hayashi Y., Kashiwagi M., Yasuda K., Ando R., Kanuka M., Sakai K., et al. (2015) **Cells of a common developmental origin regulate REM/non-REM sleep and wakefulness in mice** *Science* **350**:957–961 https://doi.org/10.1126/science.aad1023

Jego S., Glasgow S. D., Herrera C. G., Ekstrand M., Reed S. J., Boyce R., et al. (2013) **Optogenetic identification of a rapid eye movement sleep modulatory circuit in the hypothalamus** *Nat. Neurosci* **16**:1637–1643 https://doi.org/10.1038/nn.3522

John J., Wu M.-F., Boehmer L. N., Siegel J. M (2004) **Cataplexy-Active Neurons in the Hypothalamus: Implications for the Role of Histamine in Sleep and Waking Behavior** *Neuron* **42**:619–634 https://doi.org/10.1016/S0896-6273(04)00247-8

Kroeger D., Absi G., Gagliardi C., Bandaru S. S., Madara J. C., Ferrari L. L., et al. (2018) **Galanin neurons in the ventrolateral preoptic area promote sleep and heat loss in mice** *Nat. Commun* **9** https://doi.org/10.1038/s41467-018-06590-7

Lin J.-S., Sakai K., Jouvet M (1988) **Evidence for histaminergic arousal mechanisms in the hypothalamus of cat** *Neuropharmacology* **27**:111–122 https://doi.org/10.1016/0028-3908(88)90159-1

Lu J., Greco M. A., Shiromani P., Saper C. B (2000) **Effect of lesions of the ventrolateral preoptic nucleus on NREM and REM sleep** *J. Neurosci. Off. J. Soc. Neurosci* **20**:3830–3842 https://doi.org/10.1523/JNEUROSCI.20-10-03830.2000

Lu J., Bjorkum A. A., Xu M., Gaus S. E., Shiromani P. J., Saper C. B (2002) **Selective activation of the extended ventrolateral preoptic nucleus during rapid eye movement sleep** *J. Neurosci. Off. J. Soc. Neurosci* **22**:4568–4576 https://doi.org/10.1523/JNEUROSCI.22-11-04568.2002

Ma Y., Miracca G., Yu X., Harding E. C., Miao A., Yustos R., et al. (2019) **Galanin Neurons Unite Sleep Homeostasis and α2-Adrenergic Sedation** *Curr. Biol. CB* **29**:3315–3322 https://doi.org/10.1016/j.cub.2019.07.087

McGinty D. J., Sterman M. B (1968) **Sleep suppression after basal forebrain lesions in the cat** *Science* **160**:1253–1255 https://doi.org/10.1126/science.160.3833.1253

Miracca G., Anuncibay-Soto B., Tossell K., Yustos R., Vyssotski A. L., Franks N. P., et al. (2022) **NMDA Receptors in the Lateral Preoptic Hypothalamus Are Essential for Sustaining NREM and REM Sleep** *J. Neurosci. Off. J. Soc. Neurosci* **42**:5389–5409 https://doi.org/10.1523/JNEUROSCI.0350-21.2022

Nauta W. J. H (1946) **Hypothalamic regulation of sleep in rats; an experimental study** *J. Neurophysiol* **9**:285–316 https://doi.org/10.1152/jn.1946.9.4.285

Osaka T., Matsumura H (1995) **Noradrenaline inhibits preoptic sleep-active neurons through alpha 2-receptors in the rat** *Neurosci. Res* **21**:323–330 https://doi.org/10.1016/0168-0102(94)00871-c

Osorio-Forero A., Foustoukos G., Cardis R., Cherrad N., Devenoges C., Fernandez L. M. J., et al. (2023) **Osorio-Forero, A., Foustoukos, G., Cardis, R., Cherrad, N., Devenoges, C., Fernandez, L. M. J., et al. (2023). Locus coeruleus activity fluctuations set a non-reducible timeframe for mammalian NREM-REM sleep cycles. 2023.05.20.541586. doi: 10.1101/2023.05.20.541586.** *Locus coeruleus activity fluctuations set a non-reducible timeframe for mammalian NREM-REM sleep cycles* **2023** https://doi.org/10.1101/2023.05.20.541586

Palagini L., Baglioni C., Ciapparelli A., Gemignani A., Riemann D (2013) **REM sleep dysregulation in depression: state of the art** *Sleep Med. Rev* **17**:377–390 https://doi.org/10.1016/j.smrv.2012.11.001

Panula P., Yang H. Y., Costa E (1984) **Histamine-containing neurons in the rat hypothalamus** *Proc. Natl. Acad. Sci. U. S. A* **81**:2572–2576 https://doi.org/10.1073/pnas.81.8.2572

Rechtschaffen A., Bergmann B. M., Gilliland M. A., Bauer K (1999) **Effects of method, duration, and sleep stage on rebounds from sleep deprivation in the rat** *Sleep* **22**:11–31 https://doi.org/10.1093/sleep/22.1.11

Ross R. J., Ball W. A., Sullivan K. A., Caroff S. N (1989) **Sleep disturbance as the hallmark of posttraumatic stress disorder** *Am. J. Psychiatry* **146**:697–707 https://doi.org/10.1176/ajp.146.6.697

Saito Y. C., Maejima T., Nishitani M., Hasegawa E., Yanagawa Y., Mieda M., et al. (2018) **Monoamines Inhibit GABAergic Neurons in Ventrolateral Preoptic Area That Make Direct Synaptic Connections to Hypothalamic Arousal Neurons** *J. Neurosci. Off. J. Soc. Neurosci* **38**:6366–6378 https://doi.org/10.1523/JNEUROSCI.2835-17.2018

Sallanon M., Denoyer M., Kitahama K., Aubert C., Gay N., Jouvet M (1989) **Long-lasting insomnia induced by preoptic neuron lesions and its transient reversal by muscimol injection into the posterior hypothalamus in the cat** *Neuroscience* **32**:669–683 https://doi.org/10.1016/0306-4522(89)90289-3

Schott A. L., Baik J., Chung S., Weber F (2023) **A medullary hub for controlling REM sleep and pontine waves** *Nat. Commun* **14** https://doi.org/10.1038/s41467-023-39496-0

Shea J. L., Mochizuki T., Sagvaag V., Aspevik T., Bjorkum A. A., Datta S (2008) **Rapid eye movement (REM) sleep homeostatic regulatory processes in the rat: changes in the sleep-wake stages and electroencephalographic power spectra** *Brain Res* **1213**:48–56 https://doi.org/10.1016/j.brainres.2008.03.062

Sherin J. E., Shiromani P. J., McCarley R. W., Saper C. B (1996) **Activation of Ventrolateral Preoptic Neurons During Sleep** *Science* **271**:216–219 https://doi.org/10.1126/science.271.5246.216

Siegel J., Gordon T. P (1965) **PARODOXICAL SLEEP: DEPRIVATION IN THE CAT** *Science* **148**:978–980 https://doi.org/10.1126/science.148.3672.978

Smith J., Honig-Frand A., Antila H., Weber F., Chung S (2022) **Smith, J., Honig-Frand, A., Antila, H., Weber, F., and Chung, S. (2022). Regulation of stress-induced sleep fragmentation by preoptic glutamatergic neurons. 2022.11.30.518589. doi: 10.1101/2022.11.30.518589.** *Regulation of stress-induced sleep fragmentation by preoptic glutamatergic neurons* **2022** https://doi.org/10.1101/2022.11.30.518589

Steininger T. L., Alam Md, Gong N., Szymusiak H., and McGinty R. (1999) **Sleep–waking discharge of neurons in the posterior lateral hypothalamus of the albino rat** *Brain Res* **840**:138–147 https://doi.org/10.1016/S0006-8993(99)01648-0

Steininger T. L., Gong H., McGinty D., Szymusiak R (2001) **Subregional organization of preoptic area/anterior hypothalamic projections to arousal-related monoaminergic cell groups** *J. Comp. Neurol* **429**:638–653

Stucynski J. A., Schott A. L., Baik J., Chung S., Weber F (2022) **Regulation of REM sleep by inhibitory neurons in the dorsomedial medulla** *Curr. Biol* **32**:37–50 https://doi.org/10.1016/j.cub.2021.10.030

Szymusiak R., Alam N., Steininger T. L., McGinty D (1998) **Sleep-waking discharge patterns of ventrolateral preoptic/anterior hypothalamic neurons in rats** *Brain Res* **803**:178–188 https://doi.org/10.1016/s0006-8993(98)00631-3

Takahashi K., Lin J.-S., Sakai K (2006) **Neuronal Activity of Histaminergic Tuberomammillary Neurons During Wake–Sleep States in the Mouse** *J. Neurosci* **26**:10292–10298 https://doi.org/10.1523/JNEUROSCI.2341-06.2006

Takahashi K., Lin J.-S., Sakai K (2009) **Characterization and mapping of sleep-waking specific neurons in the basal forebrain and preoptic hypothalamus in mice** *Neuroscience* **161**:269–292 https://doi.org/10.1016/j.neuroscience.2009.02.075

Tervo D. G. R., Hwang B.-Y., Viswanathan S., Gaj T., Lavzin M., Ritola K. D., et al. (2016) **A Designer AAV Variant Permits Efficient Retrograde Access to Projection Neurons** *Neuron* **92**:372–382 https://doi.org/10.1016/j.neuron.2016.09.021

Torontali Z. A., Fraigne J. J., Sanghera P., Horner R., Peever J (2019) **The Sublaterodorsal Tegmental Nucleus Functions to Couple Brain State and Motor Activity during REM Sleep and Wakefulness** *Curr. Biol. CB* **29**:3803–3813 https://doi.org/10.1016/j.cub.2019.09.026

Van Dort C. J., Zachs D. P., Kenny J. D., Zheng S., Goldblum R. R., Gelwan N. A., et al. (2015) **Optogenetic activation of cholinergic neurons in the PPT or LDT induces REM sleep** *Proc. Natl. Acad. Sci. U. S. A* **112**:584–589 https://doi.org/10.1073/pnas.1423136112

Vanni-Mercier G., Gigout S., Debilly G., Lin J. S (2003) **Waking selective neurons in the posterior hypothalamus and their response to histamine H3-receptor ligands: an electrophysiological study in freely moving cats** *Behav. Brain Res* **144**:227–241 https://doi.org/10.1016/s0166-4328(03)00091-3

Verret L., Fort P., Gervasoni D., Léger L., Luppi P.-H (2006) **Localization of the neurons active during paradoxical (REM) sleep and projecting to the locus coeruleus noradrenergic neurons in the rat** *J. Comp. Neurol* **495**:573–586 https://doi.org/10.1002/cne.20891

Von Economo C. (1930) **Sleep as a problem of localization** *J. Nerv. Ment. Dis* **71**:249–259 https://doi.org/10.1097/00005053-193003000-00007

Watanabe T., Taguchi Y., Hayashi H., Tanaka J., Shiosaka S., Tohyama M., et al. (1983) **Evidence for the presence of a histaminergic neuron system in the rat brain: an immunohistochemical analysis** *Neurosci. Lett* **39**:249–254 https://doi.org/10.1016/0304-3940(83)90308-7

Weber F., Machens C. K., Borst A (2010) **Spatiotemporal response properties of optic-flow processing neurons** *Neuron* **67**:629–642 https://doi.org/10.1016/j.neuron.2010.07.017

Weber F., Chung S., Beier K. T., Xu M., Luo L., Dan Y (2015) **Control of REM sleep by ventral medulla GABAergic neurons** *Nature* **526**:435–438 https://doi.org/10.1038/nature14979

Weber F., Hoang Do J. P., Chung S., Beier K. T., Bikov M., Saffari Doost M., et al. (2018) **Regulation of REM and Non-REM Sleep by Periaqueductal GABAergic Neurons** *Nat. Commun* **9** https://doi.org/10.1038/s41467-017-02765-w

Williams R. H., Chee M. J. S., Kroeger D., Ferrari L. L., Maratos-Flier E., Scammell T. E., et al. (2014) **Optogenetic-mediated release of histamine reveals distal and autoregulatory mechanisms for controlling arousal** *J. Neurosci. Off. J. Soc. Neurosci* **34**:6023–6029 https://doi.org/10.1523/JNEUROSCI.4838-13.2014

Zhang Y., Rózsa M., Liang Y., Bushey D., Wei Z., Zheng J., et al. (2023) **Fast and sensitive GCaMP calcium indicators for imaging neural populations** *Nature* **615**:884–891 https://doi.org/10.1038/s41586-023-05828-9

Zhang Z., Ferretti V., Güntan İ., Moro A, Steinberg E. A., Ye Z, et al. (2015) **Neuronal ensembles sufficient for recovery sleep and the sedative actions of α2 adrenergic agonists** *Nat. Neurosci* **18**:553–561 https://doi.org/10.1038/nn.3957

Article and author information

John Maurer
Department of Neuroscience, Chronobiology and Sleep Institute, Perelman School of Medicine, University of Pennsylvania, Philadelphia, PA 19104, USA
ORCID iD: 0000-0003-2710-1963

Alex Lin
Department of Neuroscience, Chronobiology and Sleep Institute, Perelman School of Medicine, University of Pennsylvania, Philadelphia, PA 19104, USA

Xi Jin
Department of Neuroscience, Chronobiology and Sleep Institute, Perelman School of Medicine, University of Pennsylvania, Philadelphia, PA 19104, USA

Jiso Hong
Department of Neuroscience, Chronobiology and Sleep Institute, Perelman School of Medicine, University of Pennsylvania, Philadelphia, PA 19104, USA

Nicholas Sathi
Department of Neuroscience, Chronobiology and Sleep Institute, Perelman School of Medicine, University of Pennsylvania, Philadelphia, PA 19104, USA

Romain Cardis
Department of Fundamental Neurosciences, University of Lausanne, Rue du Bugnon 9, CH-1005 Lausanne, Switzerland

Alejandro Osorio-Forero
Department of Fundamental Neurosciences, University of Lausanne, Rue du Bugnon 9, CH-1005 Lausanne, Switzerland

Anita Lüthi
Department of Fundamental Neurosciences, University of Lausanne, Rue du Bugnon 9, CH-1005 Lausanne, Switzerland

Franz Weber
Department of Neuroscience, Chronobiology and Sleep Institute, Perelman School of Medicine, University of Pennsylvania, Philadelphia, PA 19104, USA
ORCID iD: 0000-0002-4541-4907

Shinjae Chung
Department of Neuroscience, Chronobiology and Sleep Institute, Perelman School of Medicine, University of Pennsylvania, Philadelphia, PA 19104, USA
For correspondence: shinjaec@pennmedicine.upenn.edu
ORCID iD: 0000-0003-2268-563X

Copyright

Editors

Reviewing Editor
Adrien Peyrache
McGill University, Montreal, Canada

Senior Editor
Laura Colgin
University of Texas at Austin, Austin, United States of America

Reviewer #1 (Public Review):

Summary:
This paper identifies GABA cells in the preoptic hypothalamus which are involved in REM sleep rebound (the increase in REM sleep) after selective REM sleep deprivation. By calcium

photometry, these cells are most active during REM, and show more claim signals during REM deprivation, suggesting they respond to "REM pressure". Inhibiting these cells ontogenetically diminishes REM sleep. The optogenetic and photometry work is carried out to a high standard, the paper is well-written, and the findings are interesting.

Points that could be addressed or discussed:
1. The circuit mechanism for REM rebound is not defined. How do the authors see REM rebound as working from the POAGAD2 cells? Although the POAGAD2 does project to the TMN, the actual REM rebound could be mediated by a projection of these cells elsewhere. This could be discussed.

2. The "POAGAD2 to TMN" name for these cells is somewhat confusing. The authors chose this name because they approach the POAGAD2 cells via retrograde AAV labelling (rAAV injected into the TMN). However, the name also seems to imply that neurons (perhaps histamine neurons) in the TMN are involved in the REM rebound, but there is no evidence in the paper that this is the case. Although it is nice to see from the photometry studies that the histamine cells are selectively more active (as expected) in NREM sleep (Fig. S2), I could not logically see how this was a relevant finding to REM rebound or the subject of the paper. There are many other types of cells in the TMN area, not just histamine cells, so are the authors suggesting that these non-histamine cells in the TMN could be involved?

3. It is a puzzle why most of the neurons in the POA seem to have their highest activity in REM, as also found by Miracca et al 2022, yet presumably some of these cells are going to be involved in NREM sleep as well. Could the same POAGAD2-TMN cells identified by the authors also be involved in inducing NREM sleep-inhibiting histamine neurons (Chung et al). And some of these POA cells will also be involved in NREM sleep homeostasis (e.g. Ma et al Curr Biol)? Is NREM sleep rebound necessary before getting REM sleep rebound? Indeed, can these two things (NREM and REM sleep rebound) be separated?

4. Is it possible to narrow down the POA area where the GAD2 cells are located more precisely?

5. It would be ideal to further characterize these particular GAD2 cells by RT-PCR or RNA seq. Which other markers do they express?

- https://doi.org/10.7554/eLife.92095.1.sa1

Reviewer #2 (Public Review):

Maurer et al investigated the contribution of GAD2+ neurons in the preoptic area (POA), projecting to the tuberomammillary nucleus (TMN), to REM sleep regulation. They applied an elegant design to monitor and manipulate the activity of this specific group of neurons: a GAD2-Cre mouse, injected with retrograde AAV constructs in the TMN, thereby presumably only targeting GAD2+ cells projecting to the TMN. Using this set-up in combination with technically challenging techniques including EEG with photometry and REM sleep deprivation, the authors found that this cell-type studied becomes active shortly (≈40sec) prior to entering REM sleep and remains active during REM sleep. Moreover, optogenetic inhibition of GAD2+ cells inhibits REM sleep by a third and also impairs the rebound in REM sleep in the following hour. Despite a few reservations or details that would benefit from further clarification (outlined below), the data makes a convincing case for the role of GAD2+ neurons in the POA projecting to the TMN in REM sleep regulation.

The authors found that optogenetic inhibition of GAD2+ cells suppressed REM sleep in the hour following the inhibition (e.g. Fig2 and Fig4). If the authors have the data available, it would be important to include the subsequent hours in the rebound time (e.g. from ZT8.5 to ZT24) to test whether REM sleep rebound remains impaired, or recovers, albeit with a delay.

REM sleep is under tight circadian control (e.g. Wurts et al., 2000 in rats; Dijk, Czeisler 1995 in humans). To contextualize the results, it would be important to mention that it is not clear if the role of the manipulated neurons in REM sleep regulation hold at other circadian times of the day.

The effect size of the REM sleep deprivation using the vibrating motor method is unclear. In FigS4-D, the experimental mice reduce their REM sleep to 3% whereas the control mice spend 6% in REM sleep. In Fig4, mice are either subjected to REM sleep deprivation with the vibrating motor (controls), or REM sleep deprivations + optogenetics (experimental mice). The control mice (vibrating motor) in Fig4 spend 6% of their time in REM sleep, which is double the amount of REM sleep compared to the mice receiving the same treatment in FigS4-D. Can the authors clarify the origin of this difference in the text?

- https://doi.org/10.7554/eLife.92095.1.sa0